JCB Journal of Cell Biology

REPORT

Interferon-stimulated gene 15 accelerates replication fork progression inducing chromosomal breakage

Maria Chiara Raso[1], Nikola Djoric[1], Franziska Walser[1], Sandra Hess[2], Fabian Marc Schmid[1], Sibylle Burger[1], Klaus-Peter Knobeloch[2], and Lorenza Penengo[1]

DNA replication is highly regulated by the ubiquitin system, which plays key roles upon stress. The ubiquitin-like modifier ISG15 (interferon-stimulated gene 15) is induced by interferons, bacterial and viral infection, and DNA damage, but it is also constitutively expressed in many types of cancer, although its role in tumorigenesis is still largely elusive. Here, we show that ISG15 localizes at the replication forks, in complex with PCNA and the nascent DNA, where it regulates DNA synthesis. Indeed, high levels of ISG15, intrinsic or induced by interferon-β, accelerate DNA replication fork progression, resulting in extensive DNA damage and chromosomal aberrations. This effect is largely independent of ISG15 conjugation and relies on ISG15 functional interaction with the DNA helicase RECQ1, which promotes restart of stalled replication forks. Additionally, elevated ISG15 levels sensitize cells to cancer chemotherapeutic treatments. We propose that ISG15 up-regulation exposes cells to replication stress, impacting genome stability and response to genotoxic drugs.

Introduction

Timely and accurate DNA replication in dividing cells is crucial to maintain the integrity of the human genome. However, due to constitutive growth signaling and defective DNA repair, cancer cells may exhibit replication stress, a phenomenon characterized by perturbation of error-free DNA replication and slowing or stalling of replication fork progression and DNA synthesis, inducing genomic instability and tumorigenesis (Zeman and Cimprich, 2014). Replication stress can arise as consequence of normal cellular events involving DNA (i.e., replication–transcription collisions and replication of special DNA structures, such as telomeres, fragile sites, and G-quadruplex), upon exposure to external agents, including irradiation or chemotherapeutic drugs, or after oncogene activation (Muñoz and Méndez, 2017). Although replication stress has been proven to induce genomic instability and tumorigenesis, recent studies have shown that enhancing replicative stress to induce catastrophic failure of cancer cell proliferation may provide a powerful therapeutic approach (Forment and O'Connor, 2018).

The mechanisms that underlie the cellular DNA damage response and DNA replication stress are complex and tightly controlled by posttranslational protein modifications, including phosphorylation, acetylation, methylation, poly-(ADP-ribosyl)ation, and modifications by the ubiquitin system (Wang et al., 2017). Ubiquitin-like modifiers (UBLs) are small polypeptides whose three-dimensional structures are strikingly similar to that of ubiquitin, although the similarity in their amino acid sequences to ubiquitin significantly varies (Kerscher et al., 2006). Ubiquitin and UBLs have pivotal roles in the cellular response to various forms of stress and mainly act via covalent conjugation to target proteins. This kind of protein modification can affect stability, subcellular localization, activity, and overall function (Wang et al., 2017). The role of ubiquitin and the UBLs SUMO and NEDD8 in the control of cell cycle and DNA damage response has been extensively studied (Brown and Jackson, 2015; Dantuma and van Attikum, 2016). However, the function of most UBLs, including ISG15 (the first UBL identified), in genome stability is largely unknown.

As part of the innate immunity, *ISG15* is robustly induced by type I and III IFNs, in order to protect the host during pathogen infection (Loeb and Haas, 1992; Perng and Lenschow, 2018). ISG15 can modify many cellular proteins, in a process called ISGylation, by conjugating its C-terminal glycine residue to lysines on the targets, yet the fate of this modification is still largely unknown. Increasing evidence suggests that ISG15 can regulate host response also by acting as a free intracellular molecule. An example is the stabilization of USP18 by noncovalent binding of ISG15, which is essential to prevent aberrant IFN signaling in humans (Zhang et al., 2015). Furthermore,

[1]Institute of Molecular Cancer Research, University of Zurich, Zurich, Switzerland; [2]Institute of Neuropathology, University of Freiburg, Freiburg, Germany.

Correspondence to Lorenza Penengo: penengo@imcr.uzh.ch.

unconjugated ISG15 can be secreted and function as a cytokine (D'Cunha et al., 1996; Dos Santos and Mansur, 2017; Swaim et al., 2017). *ISG15* expression can also be induced independently of IFNs via the activity of p53 upon exposure to DNA-damaging agents and irradiation or in condition of telomere shortening (Jeon et al., 2012; Liu et al., 2004; Lou et al., 2009; Park et al., 2016; Park et al., 2014). Interestingly, it was shown that reversible PCNA ISGylation relays a signaling pathway to turn off error-prone translesion synthesis after DNA lesion bypass for suppressing UV-induced mutagenesis as well as for resuming normal DNA replication (Park et al., 2014).

Elevated levels of *ISG15* expression occur in many types of cancer (Andersen et al., 2006; Bektas et al., 2008; Desai et al., 2006, 2012; Ina et al., 2010; Jinawath et al., 2004; Laljee et al., 2013; Li et al., 2014; Padovan et al., 2002; Talvinen et al., 2006), and in some cases, the robust expression of *ISG15* was reported to support tumor growth (Burks et al., 2014; Forys et al., 2014; Hadjivasiliou, 2012). In spite of the increasing interest on ISG15 and its clear correlation with human malignancies, its role in tumorigenesis is still controversial and largely unexplored (Han et al., 2018; Villarroya-Beltri et al., 2017), and its mechanism of action is far from being clarified.

Here, we show that high levels of *ISG15* expression, which occur upon type I IFN (IFN-β) treatment and in many human tumors, are detrimental for the cell, leading to accelerated and deregulated DNA replication fork progression, which ultimately results in extensive chromosomal lesions. This effect is largely independent of ISG15 conjugation activity and relies on the noncovalent functional interaction with RECQ1, a key helicase involved in replication fork restart after stalling.

Results and discussion

ISG15 is localized at the DNA replication forks

To gain insight into the potential effect of ISG15 in the regulation of genome stability, we developed different systems to modulate ISG15 expression. To reproduce conditions of high levels of *ISG15* expression irrespective of IFN stimulation, we generated a human osteosarcoma (U2OS) Flp-In T-REx (FIT) cell line, which inducibly expresses FLAG-ISG15 upon doxycycline treatment. In this cell system, ISG15 levels upon induction are comparable to those observed upon IFN-β treatment (Fig. 1 A). Moreover, we established *ISG15* knockout (KO) in U2OS FIT cell lines (referred as U2OS FIT ISG15/KO) via CRISPR/Cas9-based genome editing (Fig. S1, A and B), to use as control in different experiments.

To assess the localization of ISG15 in cells, we performed subcellular fractionation and found that ISG15 is detectable not only in cytosolic and nuclear soluble fractions but also in chromatin fractions (Fig. S1 C). To validate the presence of ISG15 in chromatin compartments, we employed the isolation of proteins on nascent DNA (iPOND) technique, which allows the isolation of proteins bound, directly or indirectly, to nascent DNA at the replication forks (Sirbu et al., 2011). Using this method, we were able to confirm the localization of ISG15 on chromatin (Fig. 1 B; 5-ethynyl-2-deoxyuridine [EdU] +Thy chase, +click) and, most important, at the replication forks (Fig. 1 B; EdU +click). Finally, we adopted a cell-based method, namely the proximity ligation assay (PLA), to visualize and measure the localization of ISG15 at the replication forks by monitoring the close association of ISG15 with the proliferating cell nuclear antigen (PCNA) and newly synthesized DNA, labeled by EdU. Quantitative imaging allowed us to evaluate the high number of PLA signals (measured as foci counts per nucleus) for ISG15/PCNA and ISG15/EdU in cells expressing high levels of FLAG-ISG15 (Fig. 1, C–F). Interestingly, low ISG15/PCNA PLA signal appeared also in control cells (empty vector [EV]) likely unveiling the interaction of PCNA with endogenous ISG15, which is expressed at low basal levels in U2OS cells. Accordingly, ISG15/PCNA PLA signals are absent in the EV sample when the FLAG antibody is used instead of ISG15 antibody (Fig. S1 D). Importantly, no signal was detected in *ISG15* KO cells or upon staining with single antibodies (recognizing PCNA, ISG15, or EdU), confirming the specificity of the system (Fig. 1, D and F). These results reveal that ISG15 localizes on chromatin at the replication forks, suggesting a possible function in modulating DNA replication.

High levels of ISG15 accelerate DNA replication fork progression

To determine whether ISG15 plays a role in DNA replication, we labeled newly replicated DNA by providing cells with halogenated nucleotides and performed the DNA fiber spreading assay (Jackson and Pombo, 1998) in different experimental conditions to evaluate replication fork progression at the single-molecule level. Strikingly, cells expressing high levels of ISG15 exhibited longer newly replicated tracks during the labeling period (ISG15 + doxycycline) compared with control cells (EV, – doxycycline and + doxycycline; Fig. 1 G). In line with this, by measuring EdU incorporation in S phase using FACS, we observed an increased rate of DNA synthesis in cells with high levels of ISG15, without affecting the frequency of origin firings (Fig. S1, E and F). While analyzing replication forks that diverge from the same replication origin, we observed no fork asymmetry, which is indicative of frequent fork pausing usually associated with replication stress, as observed upon mild treatment with the topoisomerase-1 inhibitor camptothecin (CPT; 50 nM; Fig. S1, G and H). The effect of ISG15 levels on DNA replication is dose dependent and already detectable at early time points of doxycycline induction (4 and 8 h; Fig. 1, H and I). Importantly, high levels of ISG15 do not induce expression or stabilization of its deconjugating enzyme USP18 at the mRNA or protein level (data not shown), thereby excluding any contribution of USP18 to the replication phenotype observed. Taken together, these data show that ISG15 is located at DNA replication forks, where it increases the fork progression rate in a dose-dependent manner.

IFN-β treatment increases DNA replication fork progression through *ISG15* induction

Since type I IFN is one of the main physiological inducers of *ISG15* expression, we tested the effects of IFN-β stimulation on DNA replication in U2OS cells. To prevent the cytotoxic effects of IFNs on cell viability, we limited the treatment to 2 h and then chased in IFN-β–free media for different time points, tested the

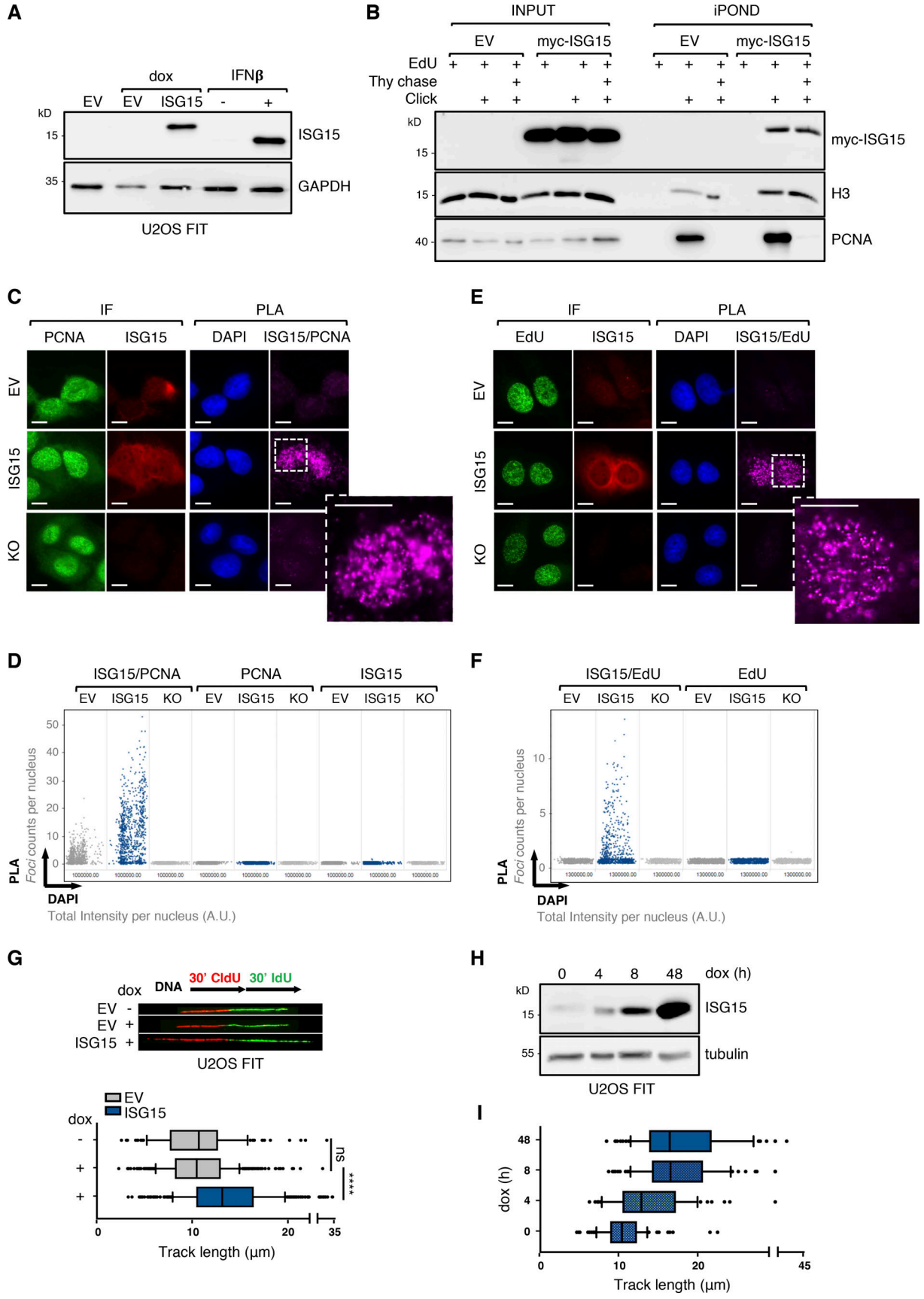

Figure 1. **ISG15 localizes at the DNA replication forks and accelerates replication fork progression. (A)** ISG15 immunoblot on protein extracts of U2OS FIT cells bearing EV or FLAG-ISG15, induced with doxycycline (dox; 1 μg/ml) for 48 h, and in parental U2OS treated with IFN-β (30 U/ml for 2 h) and chased in

medium without IFN-β for 46 h before lysis. GAPDH immunoblotting is used to normalize protein loading. **(B)** Analysis of proteins associated with nascent DNA, isolated by iPOND. HEK293T cells transfected with EV or myc-ISG15 for 24 h were pulse-labeled with EdU for 10 min and then chased with thymidine for 60 min. Immunoblotting with the indicated antibodies reveals the presence of ISG15 on chromatin (H3-positive fraction) and at the replication forks (H3- and PCNA-positive fraction). **(C)** Representative images of ISG15 colocalization with PCNA (ISG15/PCNA), as revealed by PLA. Immunofluorescence (IF) shows protein expression and cellular distribution of ISG15 and PCNA in U2OS FIT cells (treated with 1 µg/ml doxycycline for 48 h). Scale bars, 10 µm. **(D)** QIBC shows the distribution of PLA foci counts of samples described in C. For each condition, images containing ≥1,000 cells per experiment were acquired (n = 3). **(E)** Representative images of ISG15 colocalization with newly synthesized DNA (ISG15/EdU), labeled by the nucleotide analogue EdU (1 µM, 8 min), as revealed by PLA. Immunofluorescence (IF) shows cellular distribution of ISG15 and EdU in U2OS FIT cells (treated with 1 µg/ml doxycycline for 48 h). Scale bars, 10 µm. **(F)** QIBC shows the distribution of PLA foci counts of samples described in E. For each condition, images containing ≥1,000 cells per experiment were acquired (n = 3). **(G)** Top: DNA fibers labeling strategy and representative image. Bottom: Analysis of IdU track length measurements in U2OS FIT cells expressing EV or FLAG-ISG15 (treated with 1 µg/ml doxycycline for 48 h). At least 100 tracks were scored per sample (n = 5). Vertical lines represent the median value, and boxes and whiskers show 10–90th percentiles. Statistical analysis according to Mann–Whitney test; ns, not significant; ****, P < 0.0001. **(H)** FLAG-ISG15 expression in U2OS FIT cells after induction with 1 µg/ml doxycycline for the indicated time points. **(I)** Analysis of IdU track length measurements in U2OS FIT cells upon ISG15 induction as in H. At least 100 tracks were scored per sample (n = 3).

induction of *ISG15* (Fig. 2 A), and measured the rate of replication fork progression. Remarkably, we observed that treatment with IFN-β recapitulates the increased DNA replication fork speed observed in U2OS FIT cells upon doxycycline induction, which consistently correlates with *ISG15* expression levels (Fig. 2, A and B). To assess the specific contribution of ISG15 over the many factors regulated by IFNs, we tested the effect of IFN-β on replication fork progression in U2OS FIT ISG15/KO cells. Notably, we found that the accelerated fork progression rate was abrogated in cells lacking ISG15 (Fig. 2, C and D) and restored upon doxycycline-dependent reexpression of FLAG-ISG15 in U2OS FIT ISG15/KO cells (Fig. 2, E and F; see Materials and methods for details). These data clearly indicate that the increase in replication fork progression, observed upon IFN-β treatment, relies on *ISG15* expression. Additionally, to test if this is a general effect and not restricted to U2OS cells, we generated *ISG15* KO in MCF7 cells (human breast cancer; MCF7 ISG15/KO; Fig. S2 A), using the same experimental pipeline as for U2OS FIT cells, and measured replication fork progression upon IFN-β stimulation in parental (WT) and MCF7 ISG15/KO cells. In line with the data obtained in U2OS cells, we found that IFN-β accelerates fork progression in MCF7 in a ISG15-dependent manner (Fig. 2 G). Again, accelerated fork progression in MCF7 ISG15/KO cells was restored by stable reexpression of ISG15 (Fig. 2 H). Our findings provide strong evidence that accelerated DNA replication fork progression is promoted by physiological IFN-β–mediated overexpression of *ISG15*.

DNA replication fork progression in *ISG15*-expressing cancer cells relies on ISG15 levels

Since *ISG15* expression is often up-regulated in cancer, we aimed to investigate whether the rate of DNA replication is regulated by ISG15 in other cancer cells in addition to U2OS and MCF7. We analyzed the levels of ISG15 in a panel of cancer cell lines using U2OS as reference system for *ISG15* expression (Fig. S2 B). We selected three cell lines (HeLa from cervical cancer and M059K and T98G from glioblastoma) that exhibit relatively high levels of ISG15 and efficient *ISG15* knockdown upon transient transfection of siRNAs targeting *ISG15* (Figs. 2 I and S2 C). Although HeLa, M059K, and T98G cells showed intrinsic differences in DNA replication fork progression, depletion of ISG15 leads to a 30–40% reduction in replicated track length in all of these cell types (Fig. 2 J). Overall, these data show that *ISG15* expression levels affect DNA replication fork progression in cancer cells of various origin.

Accelerated replication fork progression induced by high levels of *ISG15* is largely conjugation independent

ISG15 function was mainly studied as protein modifier able to covalently conjugate to target proteins, but it can also act as free molecule by interacting with proteins noncovalently (Dos Santos and Mansur, 2017; Swaim et al., 2017; Zhang et al., 2015). To assess whether the conjugation ability of ISG15 is required for its influence on replication, we generated U2OS FIT and U2OS FIT ISG15/KO cell lines that express a mutant of *ISG15* lacking the C-terminal diglycine motif that is required for covalent modification of target proteins (ISG15ΔGG; Fig. 3 A). Overexpression of ISG15ΔGG largely recapitulated the replication phenotype observed upon overexpression of WT ISG15 (Fig. 3 B; and Fig. S3, A and B). Likewise, ISG15ΔGG also accelerated replication fork progression in the context of *ISG15* KO cells and localizes in close proximity to PCNA, as revealed by PLA analysis (FLAG/PCNA), although to a lesser extent than WT ISG15 (Fig. 3, B and C), suggesting possible additional roles for ISG15 conjugation in DNA synthesis. Analogous to WT ISG15, expression of ISG15ΔGG did not induce fork asymmetry or alterations in cell cycle distribution (Fig. S3, C and D).

ISG15 consists of two tandem ubiquitin-like domains bearing the typical β-grasp folds (Narasimhan et al., 2005), though the sequence homology with ubiquitin is quite low (Fig. S3 E). Intriguingly, while analyzing the crystal structure of ISG15, we observed that the N-terminal lobe of ISG15 contains a hydrophobic surface, centered on L10, L72, and V74 (referred as LLV), reminiscent of the hydrophobic patch characteristic for ubiquitin (L8, I44, and V70; Fig. 3 D). This patch is strictly required for ubiquitin functions and constitutes the recognition site of most ubiquitin-binding domains (Hicke et al., 2005). Therefore, we tested whether the LLV patch is required for ISG15 function. We found that single mutations in the LLV patch significantly reduced fork acceleration induced by high levels of ISG15, while the triple mutant suppressed it completely (LLVAAA; Fig. 3, E and F) without major alterations of cellular localization (Fig. S3 F). To exclude that mutations targeting the LLV patch generally affect ISG15 protein folding, we tested the ability of L72A and the LLVAAA mutants to conjugate to target proteins. When

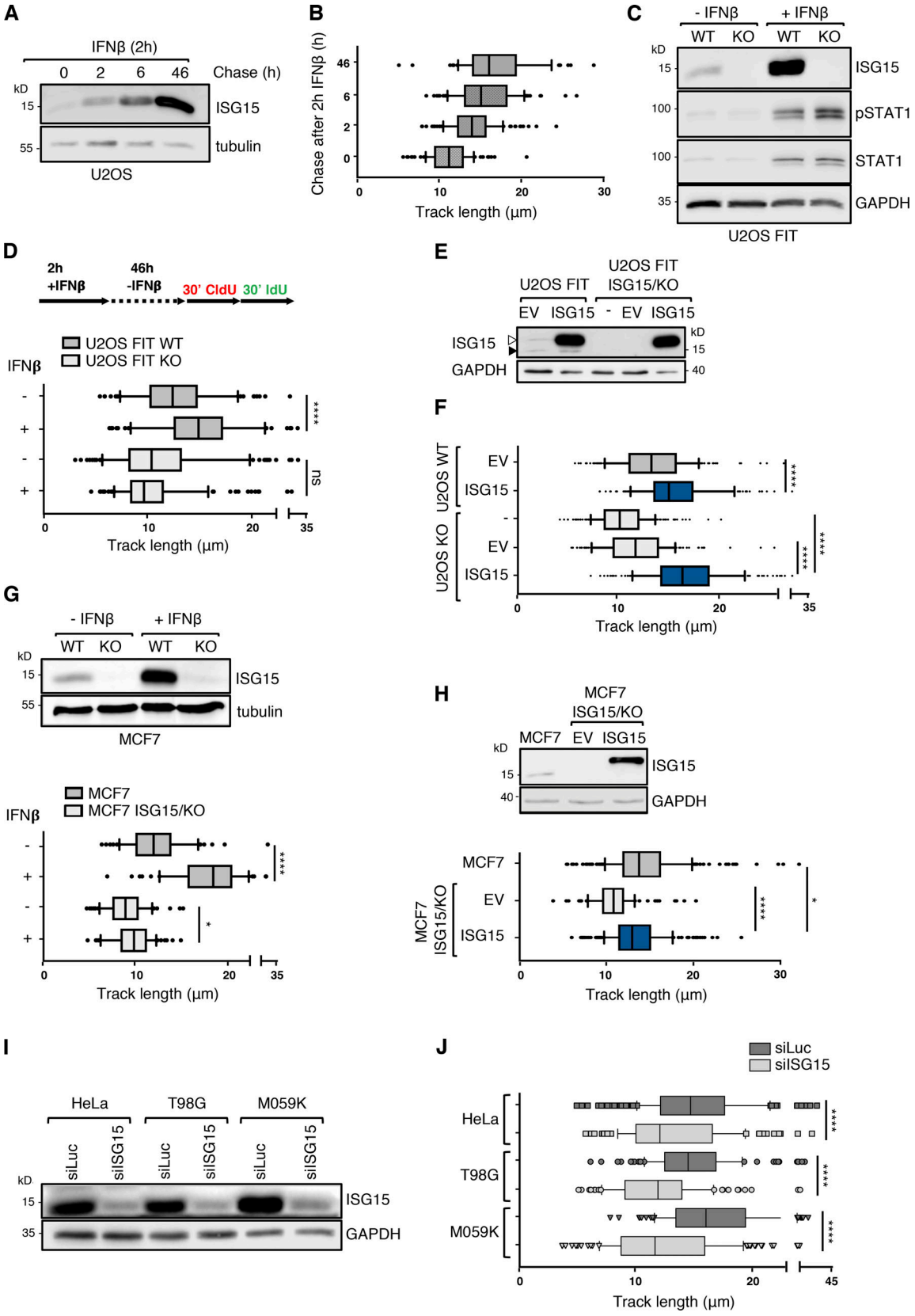

Figure 2. ***ISG15* expression levels impact on replication fork progression in different systems. (A)** Time course of *ISG15* expression in U2OS treated with IFN-β (30 U/ml, 2 h) and chased for the indicated time points before lysis. **(B)** Analysis of IdU track length measurements in U2OS cells treated with IFN-β as in A. At least 100 tracks were scored per sample (n = 3). **(C)** ISG15 protein levels in U2OS FIT cells carrying *ISG15* WT or *ISG15* KO treated with IFN-β (30 U/ml, 2 h) and chased for 46 h before lysis. Phosphorylated STAT1 (pSTAT1) reveals activation of IFN-β pathway. Immunoblot with STAT1 and GAPDH are used to

normalize protein loading. **(D)** Top: DNA fiber–labeling strategy. Bottom: Analysis of IdU track length measurements in U2OS as in C. At least 100 tracks were scored per sample (n = 3). Vertical lines represent the median value, and boxes and whiskers show 10–90th percentiles. Statistical analysis according to Mann–Whitney test; ns, not significant; ****, P < 0.0001. **(E)** ISG15 immunoblot of parental U2OS FIT cells expressing EV or FLAG-ISG15 and U2OS FIT cells lacking the endogenous *ISG15* (U2OS ISG15/KO) and reexpressing stably integrated EV or exogenous FLAG-ISG15 after 48 h induction with 1 µg/ml doxycycline. Western blot analysis reveals the expression of endogenous (black triangle) and exogenous (white triangle) *ISG15*. **(F)** Analysis of IdU track length measurements in U2OS as in (E). At least 100 tracks were scored per sample (n = 3). Vertical lines represent the median value, and boxes and whiskers show 10–90th percentiles. Statistical analysis according to Mann–Whitney test; ****, P < 0.0001. **(G)** Top: *ISG15* expression in MCF7 cells carrying *ISG15* WT or *ISG15* KO treated with IFN-β (30 U/ml, 2 h) and chased for 46 h before lysis. Bottom: Analysis of IdU track length measurements. At least 100 tracks were scored per sample (n = 3). Vertical lines represent the median value, and boxes and whiskers show 10–90th percentiles. Statistical analysis according to Mann–Whitney test; ****, P < 0.0001; *, P < 0.05. **(H)** Top: ISG15 protein levels in MCF7 cells bearing the WT gene of *ISG15* (MCF7) and cells lacking the endogenous *ISG15* (MCF7 ISG15/KO) stably integrated with EV or FLAG-ISG15. Bottom: Analysis of IdU track length measurements. At least 100 tracks were scored per sample (n = 3). Vertical lines represent the median value, and boxes and whiskers show 10–90th percentiles. Statistical analysis according to Mann–Whitney test; ****, P < 0.0001; *, P < 0.05. **(I)** *ISG15* knockdown (siISG15) 48 h after siRNA transfection in HeLa, T98G, and M059K cells. siLuc is used as control. **(J)** Analysis of IdU track length measurements as in I. At least 100 tracks were scored per sample (n = 3). Vertical lines represent the median value, and boxes and whiskers show 10–90th percentiles. Statistical analysis according to Mann–Whitney test; ****, P < 0.0001.

coexpressed in HEK293T cells together with the ISG15 conjugation machinery (UBE1L as E1, UBCH8 as E2, and HERC5 as E3), both ISG15 variants were as efficiently conjugated as WT ISG15 (Fig. S3 G).

Accelerated fork progression by ISG15 depends on the functional interaction with RECQ1

To pinpoint factors potentially involved in the replication function of ISG15, we performed mass spectrometry analysis to search for ISG15 binding partners, rather than targets, by analyzing the chromatin factors interacting with ISG15ΔGG (Fig. 3 A; and Fig. S4, A–C). Under these conditions, we found a limited number of potential interaction partners of ISG15 (Table S1). The best candidates were ranked on the basis of their function and chromatin localization. One of the most promising factors identified was RECQ1, a key DNA helicase that binds a variety of DNA structures, including DNA replication forks and Holliday junctions (Popuri et al., 2008; Sharma et al., 2005), and promotes the branch migration and restart of DNA replication forks upon fork stalling (Berti et al., 2013). To validate RECQ1 interaction, we performed coimmunoprecipitation in HEK293T cells overexpressing both HA-RECQ1 and myc-ISG15 and observed a relatively modest interaction (Fig. S4 D), while no clear association was found using recombinant proteins (data not shown), likely suggesting that ISG15–RECQ1 interaction is difficult to detect and study by standard biochemistry. Therefore, to better explore the ISG15–RECQ1 interaction, we exploited the NanoBRET assay, based on the bioluminescence resonance energy transfer optimized to study dynamic interactions between proteins in a cellular context, due to the distance constraint of energy transfer of ∼5 nm (Machleidt et al., 2015). Importantly, this assay revealed a clear association of RECQ1 with ISG15, both as WT and as conjugation-defective variant, whereas no signal was observed with p53, an unrelated protein that we used as a control for specificity (Figs. 4 B and S4 E). To further corroborate this result, we performed PLA on U2OS FIT cells expressing ISG15 WT and ISG15ΔGG using antibodies against ISG15 and endogenous RECQ1, and we obtained remarkably strong signals in both cases, providing further evidence that RECQ1 is indeed in a protein complex with ISG15 (Fig. 4, C and D).

Next, we addressed the functional link between ISG15 and RECQ1 by assessing whether the expression of *RECQ1* is required for the replication phenotype observed in cells expressing high levels of ISG15. Notably, depletion of RECQ1 completely abolished the accelerated replication fork progression induced by high levels of ISG15 and ISG15ΔGG (Fig. 4, E and F), suggesting that ISG15 may regulate RECQ1 function by unleashing its restart activity. To test whether ISG15 promotes RECQ1-dependent fork restart, we measured the DNA replication restart after fork stalling using an established DNA fiber protocol that includes a prolonged treatment with hydroxyurea (HU; 4 mM, 4 h) between nucleotide analogue–labeling periods. In line with previous results (Berti et al., 2013; Zellweger et al., 2015), RECQ1-depleted cells were only partially defective in fork restart due to the contribution of alternative restart pathways (Thangavel et al., 2015). Notably, cells expressing high levels of ISG15 display accelerated restart of stalled forks, which is suppressed by RECQ1 depletion, leading to a marked fork restart defect (Fig. 4, G and H). Collectively, these data strongly suggest that ISG15 promotes the fork restart activity of RECQ1, without affecting RECQ1 protein levels (Fig. S4 F).

High levels of ISG15 unleash DNA replication, induce DNA breakages, and sensitize cells to genotoxic stress

We next addressed whether high levels of ISG15 could also lead to unrestrained replication fork progression in conditions of mild DNA replication stress, which is typically associated with early tumorigenesis or chemotherapeutic treatments (Berti and Vindigni, 2016; Macheret and Halazonetis, 2015). Cells expressing high levels of *ISG15* and control cells were challenged by mild doses of genotoxic agents, which cause replication fork slowing without detectable DNA damage (Zellweger et al., 2015), and then subjected to DNA fiber analysis. The ratio between 5-iodo-2-deoxyuridine (IdU) and 5-chloro-2'-deoxyuridine (CldU) was measured to assess the replication slowdown observed upon treatment with genotoxic stress (see scheme in Fig. 5 A). As expected, replication fork progression was significantly reduced in control cells treated with a low dose (50 nM) of CPT (EV + CPT). In contrast, cells expressing high levels of either WT or ISG15ΔGG were less sensitive to CPT treatment and displayed unrestrained fork progression (Fig. 5 A). Similar effects were observed upon treatment with mild doses of the DNA cross-linking agent cisplatin (*cis*-diamminedichloridoplatinum(II), CDDP; 1 µM), but not with HU (0.5 mM), which, at this

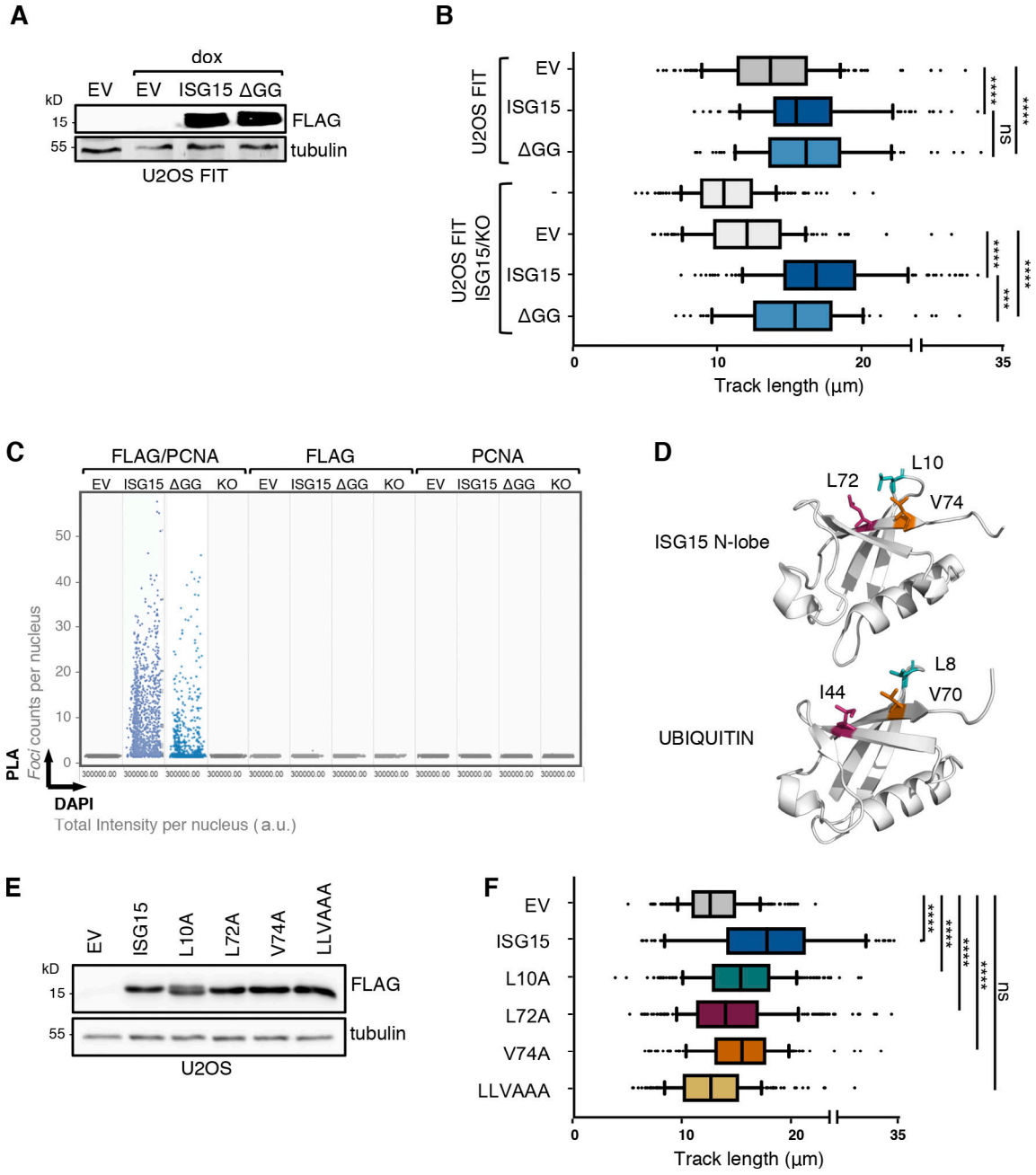

Figure 3. **Accelerated replication fork progression in cells expressing high levels of ISG15 is largely conjugation independent. (A)** ISG15 immunoblot of U2OS FIT cells bearing EV, FLAG-ISG15, or FLAG-ISG15ΔGG after 48-h induction with 1 μg/ml doxycycline (dox). **(B)** The effect of ISG15 on DNA replication was assessed by using DNA fiber assay in parental U2OS FIT cells (as in A) and U2OS FIT cells (*ISG15* KO [U2OS ISG15/KO]; see Fig. S3 A) expressing EV, FLAG-ISG15, or FLAG-ISG15ΔGG after doxycycline induction (1 μg/ml, 48 h). At least 100 tracks were scored per sample (n = 3). Vertical lines represent the median value, and boxes and whiskers show 10–90th percentiles. Statistical analysis according to Mann–Whitney test; ns, not significant; ****, $P < 0.0001$; ***, $P < 0.001$. **(C)** Colocalization of FLAG-ISG15 and FLAG-ISG15ΔGG with PCNA (FLAG/PCNA) in U2OS FIT cells induced for 48 h with 1 μg/ml doxycycline determined by PLA. QIBC shows the distribution of PLA foci counts. For each condition, images containing ≥1,000 cells per experiment were acquired (n = 3). **(D)** Representation of 3D structure of N-terminal ubiquitin-like domain (N-lobe) of ISG15 and ubiquitin (Protein Data Bank accession nos. 1Z2M and 1UBQ, respectively). The residues corresponding to the hydrophobic patches are indicated. **(E)** U2OS FIT cells were transfected with EV, FLAG-ISG15 wild type and ISG15 mutants carrying the indicated single amino acid substitutions (L10A, L72A, and V74A) or the combination of them (LLVAAA). **(F)** Analysis of IdU track length measurements as in E. At least 100 tracks were scored per sample (n = 3). Vertical lines represent the median value, and boxes and whiskers show 10–90th percentiles. Statistical analysis according to Mann–Whitney test; ns, not significant; ****, $P < 0.0001$.

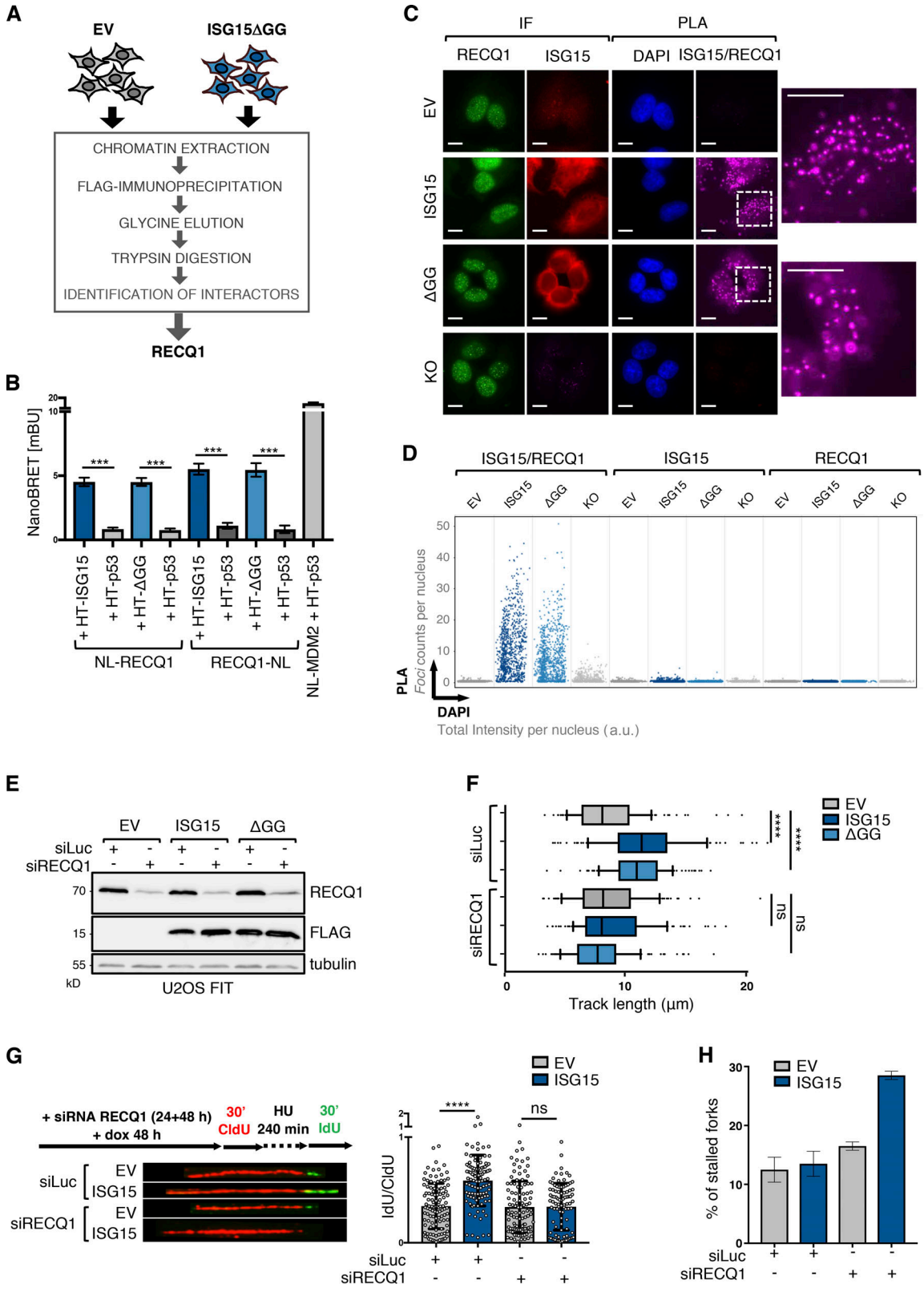

Figure 4. **Increase of replication fork progression by ISG15 depends on the functional interaction with RECQ1. (A)** Chromatin extracts were obtained from U2OS FIT cells expressing EV or FLAG-ISG15ΔGG and processed as indicated for mass spectrometry analysis. **(B)** ISG15 interaction with RECQ1 was measured as luminescence signal by NanoBRET in HEK293T cells that were cotransfected with HaloTag-Fusion constructs of ISG15 (HT-ISG15) and RECQ1 fused to NanoLuc at N-terminus (NL-RECQ1) or C-terminus (RECQ1-NL; n = 3). HT-p53 and NL-MDM2 are used as controls. **(C)** Representative images of colocalization of FLAG-ISG15 and FLAG-ISG15ΔGG with endogenous RECQ1 (ISG15/RECQ1) in U2OS FIT cells after doxycycline induction (1 μg/ml, 48 h), assessed by PLA. Scale bars, 10 μm. **(D)** QIBC shows the distribution of PLA foci counts of samples described in C. For each condition, images containing ≥1,000

cells per experiment were acquired (n = 3). **(E)** FLAG-ISG15 and RECQ1 protein levels in U2OS FIT cells expressing EV, FLAG-ISG15, or FLAG-ISG15ΔGG after doxycycline induction (1 µg/ml, 48 h) and upon knockdown of *RECQ1* by siRNA transfection. siLuc is used as control. **(F)** Analysis of IdU track length measurements as in E. At least 100 tracks were scored per sample (n = 3). Vertical lines represent the median value, and boxes and whiskers show 10–90th percentiles. Statistical analysis according to Mann–Whitney test; ns, not significant; ****, P < 0.0001. **(G)** Left: DNA fiber–labeling strategy to determine fork restart and representative images. Right: Fork restart speed (IdU) normalized on fork speed (CldU) in U2OS FIT cells upon *RECQ1* knockdown after doxycycline induction (1 µg/ml, 48 h) as described in the scheme. At least 100 tracks were scored per sample (n = 3). Statistical analysis according to Mann–Whitney test; ns, not significant; ****, P < 0.0001. **(H)** Percentage of stalled forks after HU washout in U2OS FIT cells described in G.

concentration, directly prevents fork progression by depleting nucleotides (Fig. S4 G). Remarkably, the replication rate observed in cells with high levels of ISG15 and treated with CPT was comparable to that measured in unperturbed control cells (Fig. 5 B), indicating that high ISG15 levels impose sustained fork progression even in conditions of replication stress. Moreover, the unrestrained fork progression observed in condition of high levels of ISG15 upon CPT treatment was also abrogated by loss of RECQ1 (Fig. 5 C), further suggesting that ISG15 unleashes RECQ1 restart activity, even in the context of replication stress.

Accelerated replication fork progression has been reported to be detrimental for cells (Maya-Mendoza et al., 2018). Thus, we asked whether the deregulated replication fork progression observed in context of high levels of ISG15 results into detectable genomic lesions. To address this point, we took advantage of the neutral comet assay, which allows measuring the formation of DNA double-strand breaks in different experimental conditions. Strikingly, we found that high levels of either ISG15 or ISG15ΔGG mutant were sufficient to induce the accumulation of DNA lesions in cells, and this effect was increased upon treatment with low-dose CPT (Figs. 5 D and S4 H). This adverse effect on DNA integrity is usually repaired in normal conditions. However, in cells expressing high levels of ISG15, increased chromosomal abnormalities were detected during mitosis, mostly visible as regions of decondensed chromatin along metaphase chromatids (Fig. 5, E and F). To examine whether the detrimental phenotype promoted by ISG15 impacts cell viability in response to different drugs, we performed clonogenic survival assays. Remarkably, the expression of high levels of ISG15 sensitized cells to low doses of CPT and the poly (ADP-ribose) polymerase (PARP) inhibitor (PARPi) olaparib (Fig. 5, G and H). This result supports and helps explain previous observations, showing that high levels of ISG15 increase the sensitivity to CPT in breast cancer cells (Desai et al., 2008) and correlate with high sensitivity to irinotecan (a clinically used CPT derivative) in gastric cancer (Shen et al., 2013).

Up-regulation of *ISG15* and increased ISGylation of target proteins are well-characterized IFN-mediated responses to pathogen infection (Perng and Lenschow, 2018) but are also associated with pathological conditions observed in many types of cancer. Depending on the context, either oncogenic or tumor suppressive effects were reported (Han et al., 2018). Here, we describe a novel unexpected function of the UBL ISG15 in the regulation of DNA synthesis. We demonstrate that ISG15 localizes at DNA replication forks in close proximity to PCNA and newly synthesized DNA. High levels of *ISG15* expression, as observed upon IFN induction or in our inducible cell line, deregulate replication fork progression, leading to genomic instability.

Keeping replication fork speed under tight control is essential to preserve genome stability. While slowing down replication fork progression is frequently observed when cells experience replication stress (Zeman and Cimprich, 2014), an increase in fork progression rate is far more uncommon. In the present study, we found that expression of high levels of *ISG15*, as well as its conjugation-defective form, ISG15ΔGG, causes faster and unrestrained DNA replication fork progression. In the presence of high levels of ISG15, the fork progression rate observed upon mild genotoxic stress is comparable to that of untreated control cells, strongly indicating that ISG15 dampens the active slowing of replication fork progression in response to genotoxic agents. As a result of this desensitization, cells accumulate chromosomal breakage. In line with this, we found that the rate of replication fork progression of different cancer cells constitutively expressing high levels of *ISG15* is markedly reduced upon depletion of ISG15, further supporting the role of ISG15 as a critical modulator of replication fork progression across different cellular systems.

The rate of replication fork progression may be affected by multiple factors. Since the effect of ISG15 in replication fork progression appears partly independent on its conjugation, we ran a mass spectrometric analysis searching for ISG15-interacting proteins potentially involved in the increased replication rate. Although very few chromatin-associated factors were found, three of them (RECQ1, DEK, and SMCE1) are proteins known to bind four-way junction structures, such as reversed replication forks that typically form in conditions of replication stress (Quinet et al., 2017). In the present study, we focused on the DNA helicase RECQ1, as its role in replication fork restart upon fork stalling was already established (Berti et al., 2013). Although a direct interaction between ISG15 and RECQ1 proved difficult to monitor and study, the two proteins were detected in close proximity at replication forks and displayed a clear functional interaction, as the accelerated replication fork progression induced by high ISG15 levels is fully dependent on RECQ1. However, as suggested by the mass spectrometry data, ISG15 may have a more general role in regulating DNA replication at these specific replication intermediates (i.e., the four-way junctions). Despite their close proximity, it is still unclear how ISG15 affects RECQ1's activity. Although other scenarios cannot be currently excluded, we envision that ISG15 may directly modulate the ability of RECQ1 to bind and unwind different DNA structures at stalled forks; alternatively, by binding to stalled forks, ISG15 may favor RECQ1-mediated fork restart. Further studies will need to address whether and how ISG15 regulates formation, stability, and/or restart of reversed replication forks and whether additional factors are involved.

The detrimental effects of high ISG15 levels on DNA replication and genome stability recall recent data showing a high speed of fork progression upon PARPi (Maya-Mendoza et al.,

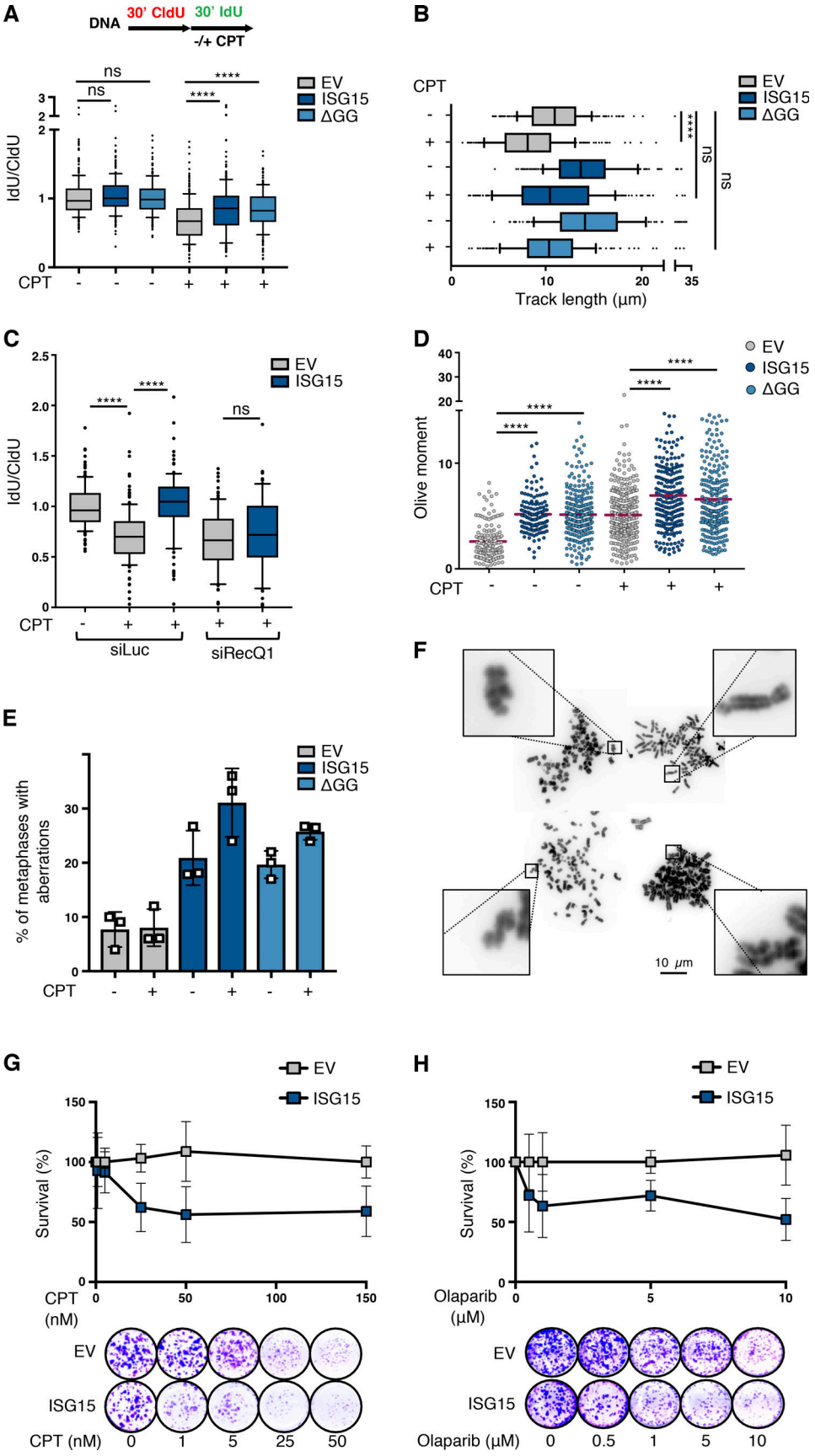

Figure 5. **High levels of ISG15 unleash DNA replication, induce DNA breakages and sensitize cells to genotoxic stress. (A)** Top: Schematic representation of DNA fiber assay strategy. Bottom: Effect of CPT treatment (50 nM), optionally added concomitantly with the second label (IdU), in U2OS FIT cells

expressing EV, FLAG-ISG15 or FLAG-ISG15ΔGG after doxycycline induction (1 µg/ml, 48 h). Drug effect (IdU + CPT) is normalized on CldU track length in untreated conditions. At least 100 tracks were scored per sample (n = 3). Horizontal lines represent the median value, and boxes and whiskers show 10–90th percentiles. Statistical analysis according to Mann–Whitney test; ns, not significant; ****, P < 0.0001. **(B)** Analysis of IdU track length measurements in cells treated as in (A). At least 100 tracks were scored per sample (n = 3). Vertical lines represent the median value, and boxes and whiskers show 10–90th percentiles. Statistical analysis according to Mann–Whitney test; ns, not significant; ****, P < 0.0001. **(C)** Effect of CPT treatment (50 nM) in U2OS FIT cells expressing EV or FLAG-ISG15 after dox-induction (1 µg/ml, 48 h) and upon *RECQ1* knockdown (siRECQ1). Drug effect (IdU + CPT) is normalized on CldU track length in untreated conditions. At least 100 tracks were scored per sample (n = 3). Horizontal lines represent the median value, and boxes and whiskers show 10–90th percentiles. Statistical analysis according to Mann–Whitney test; ns, not significant; ****, P < 0.0001. **(D)** Neutral comet assay to measure accumulation of DNA double strand breaks in U2OS FIT cells expressing EV, FLAG-ISG15 or FLAG-ISG15ΔGG induced with doxycycline (1 µg/ml) for 48 h and treated with CPT (50 nM; n = 3). **(E)** Quantification of chromosomal abnormalities by analysis of metaphase spreads of U2OS FIT cells expressing EV, FLAG-ISG15, or FLAG-ISG15ΔGG after doxycycline induction (1 µg/ml, 48 h) and treated with CPT (50 nM). At least 50 metaphases/sample were scored for every replicate. Each spot represents average of one replicate (n = 3). **(F)** Representative image of chromosomal abnormalities quantified in E. Scale bar of 10 µm is indicated. **(G and H)** Survival curve determined by clonogenic assay of U2OS FIT cells expressing EV or FLAG-ISG15 and treated with increasing doses of CPT (G) and the PARP inhibitor Olaparib (H). Values are normalized on untreated and EV (n = 3).

2018). Albeit not directly discussed in this report, the effect of PARPi effect on DNA replication rate also relies on deregulation of RECQ1, which is a key target of PARP1 negative regulation in this context (Berti et al., 2013). In line with this, we observed that the effect of ISG15 on replication fork progression was not further increased by treatment with PARPi (data not shown), suggesting that ISG15 and PARPi may affect replication fork progression with a similar mechanism. As also supported by recent studies using mouse models of chemoresistance (Gogola et al., 2019), PARP1-modulated function of RECQ1 in replication fork restart is emerging as a key regulatory process for the efficacy of anticancer treatments targeting replication. The increased activity of RECQ1 by high ISG15 levels may thus represent an important vulnerability that can be exploited for genotoxic anticancer treatments. Furthermore, the evaluation of ISG15 levels in tumor samples may represent a predictive parameter to stratify patients in personalized cancer therapy.

Why did cells evolve such a potentially harmful system to counteract infection? A possible safe-lock strategy resides on the limited availability of free intracellular ISG15. During pathogen infection, the activation of the IFN pathway leads to the expression of several genes, including the ISG15 conjugation machinery (E1, E2, and E3) that promotes extensive ISGylation of its target proteins and consequently reduces the free intracellular pool of ISG15. The detrimental effects may thus arise only when ISG15 expression and conjugation are uncoupled, resulting in abnormally high levels of free ISG15, which promote deregulated replication events.

Our data uncover the first physiological response (i.e., IFN-β stimulation) directly modulating the velocity of replication fork progression, via the induction of *ISG15* expression. Recent literature demonstrates that defects in processing DNA replication stalled forks lead to accumulation of cytosolic DNA and to activation of the cGAS–STING pathway, resulting in the activation of the type I IFN pathway with consequent expression of *ISG15* (Coquel et al., 2018). Thus, *ISG15* overexpression appears as central player in this emerging field, being at the same time a modulator of DNA replication fork speed and a consequence of replication stress.

Overall, ISG15 function in regulating replication fork progression and genome stability contributes to explain the complex role of the IFN system, and of ISG15 itself, in tumorigenesis and cancer therapy (Han et al., 2018). A key challenge for future studies will be to understand if ISG15, via interaction or conjugation to protein partners, plays additional roles in the maintenance of genome integrity, impacting other fundamental aspects of DNA replication and/or the DNA damage response and repair, and whether its expression levels might be used to predict sensitivity to therapeutic treatments.

Materials and methods

Chemicals and transfection reagents

Blasticidin (InvivoGen; catalog number ant-bl-1), hygromycin B (InvivoGen; catalog number ant-hg-05), doxycycline (Sigma-Aldrich; catalog number D9891), Geneticin (G418; Thermo Fischer Scientific; catalog number 10131035), EdU (Sigma-Aldrich; catalog number 900584), CldU (Sigma-Aldrich; catalog number C6891), IdU (Sigma-Aldrich; catalog number I7125-5G), ProLong Gold Antifade Reagent (Thermo Fisher Scientific; catalog number P36930), VECTASHIELD Antifade Mounting Medium (Vector Laboratories; catalog number H-1200), SYBR Gold Nucleic Acid Gel Stain (Invitrogen; catalog number S11494), CPT (Sigma-Aldrich; catalog number C9911), HU (Sigma-Aldrich; catalog number H8627), cisplatin (CDDP; Sigma-Aldrich; catalog number 232120), Nocodazole (Sigma-Aldrich; catalog number M1404), Olaparib (Selleckchem; catalog number S1060), SeaPlaque GTG Agarose (Lonza; catalog number 50111), FuGENE HD Transfection Reagent (Promega; catalog number E2311), and JetPRIME transfection reagent (Polyplus; catalog number 114–07) were used.

Cell lines and cell culture

MCF7, HeLa, T98G, M059K, and HEK293T cells were grown in DMEM, 10% FBS. The U2OS FIT cell line was grown in DMEM, 10% FBS tetracycline-free, complemented with blasticidin (10 µg/ml) and hygromycin B (100 µg/ml) when bearing integration.

Cellular fractionation

U2OS FIT cells were lysed in plates with hypotonic lysis buffer A (0.01 M Hepes, pH 7.5, 0.05 M NaCl, 0.3 M sucrose, 0.5% Triton X-100, protease inhibitor cocktail [1:100], 1 mM PMSF, 10 mM N-Ethylmaleimide (NEM), 10 µM PJ-34, and 75 µM Tannic acid) and incubated 15 min on ice. Cytosolic fraction was isolated after centrifuging for 5 min at 1,500 *g*. Samples were incubated for 10 min in nuclear lysis buffer B (0.01 M Hepes, pH 7, 0.2 M NaCl,

1 mM EDTA, 0.5% NP-40, protease inhibitor cocktail [1:100], 1 mM PMSF, 10 mM NEM, 10 µM PJ-34, and 75 µM Tannic acid). Samples were centrifuged for 2 min at 16,000 *g*, and the nuclear fractions were isolated. Pellets were resuspended in chromatin lysis buffer C (0.01 M Hepes, 0.5 M NaCl, 1 mM EDTA, 1% NP-40, protease inhibitor cocktail [1:100], 1 mM PMSF, 10 mM NEM, 10 µM PJ-34, and 75 µM Tannic acid), sonicated for 15 min at low amplitude, and centrifuged at 16,000 *g*, and the chromatin fractions were isolated from the supernatant.

Co-immunoprecipitation

HEK293T cells, transfected with plasmids coding for myc-ISG15 and HA-FLAG-RECQ1 or the EV, were lysed in YY buffer (50 mM Hepes, pH 7.5, 150 mM NaCl, 10% glycerol, 1% Triton X-100, 1 mM EDTA, and 1 mM EGTA) added with protease inhibitor cocktail, 1 mM PMSF, 10 mM NEM, 50 mM NaF, and 10 mM NaPyr, benzonase (100 U/ml). Cell extracts were incubated for 2 h at 4°C on a wheel with anti-HA resins (Sigma-Aldrich). Resins were washed four times with HNTG buffer (20 mM Hepes, pH 7.5, 150 mM NaCl, 10% glycerol, and 0.1% Triton X-100) before elution with Laemmli buffer at 95°C.

CRISPR/Cas9 knockout of ISG15

ISG15 KO was generated in U2OS FIT (Thermo Fisher Scientific; catalog number R78007) and MCF7 cells using a CRISPR/Cas9^{D10A} nickase system as described previously (Chiang et al., 2016). Short guide RNAs (sgRNAs) were designed using UCSC Genome Browser (GRCh38/hg38) mapping at the end of the gene between the intron/exon region shared among all ISG15 splice variants (chromosome 1: 1,013,559–1,013,605, 47 bp in GRCh38/hg38) using the online tools CRISPR Design (http://www.crispr.mit.edu) and WTSI Genome Editing (http://www.sanger.ac.uk/htgt/wge/). sgRNA sense (5′-TTACCATGGCTGTGGGCTGT-3′) and sgRNA antisense (5′-CAGATGTCACAGGTGGGGGG-3′; Microsynth). sgRNAs were cloned into All-in-One EGFP vector (AIO-GFP; Addgene; Steve Jackson Lab Plasmids, #74119) that was transfected into cells with FuGENE transfection reagent. GFP-positive cells were sorted by FACS and single-cell plated in 96-well plates. Clones were grown and *ISG15* expression was tested by immunoblotting. 42 and 41 single clones were screened for U2OS FIT and MCF7, respectively.

Replication fork progression by DNA fiber analysis

Asynchronous, subconfluent cells were labeled for 30 min with 30 µM of the thymidine analogue CldU and then washed with warm PBS and labeled for 30 min with 250 µM of another thymidine analogue, IdU, alone or in combination with genotoxic agents (50 nM CPT, 1 µM CDDP, or 0.5 mM HU). To evaluate fork restart, after CldU labeling, cells were released for 4 h in fresh media containing 4 mM HU, washed with PBS, and then labeled with IdU. Cells were collected in cold PBS, mixed 1:2 with unlabeled cells, and lysed for 8 min in 200 mM Tris-HCl, pH 7.5, 50 mM EDTA, and 0.5% [wt/vol] SDS directly on a glass slide. Slides were tilted at a 45°C to stretch the DNA fibers, air-dried, and fixed in 3:1 methanol/acetic acid overnight at 4°C. The DNA fibers were denatured for 80 min with 2.5 M HCl and blocked for 40 min with 2% BSA/PBS-Tween. Incorporated CldU and IdU tracks were stained for 2.5 h with anti-BrdU primary antibodies recognizing CldU (Abcam; catalog number ab6326) or IdU (BD Biosciences; catalog number 347580) and stained for 2 h with secondary antibody anti-mouse Alexa Fluor 488 (Invitrogen) and anti-rat Cy3 (Jackson ImmunoResearch; catalog number 712–166-153). Slides were mounted with ProLong Gold Antifade Reagent. Microscopy was done using an Olympus IX81 microscope with a charge-coupled device camera (Hamamatsu). To assess fork progression, IdU and CldU track length of DNA fiber molecules was measured using ImageJ64 software. Value in pixels was converted to micrometers considering the objective lens used during acquisition (63×; conversion factor: 1 pixel = 10.54 µm). Length was converted into fork speed considering that 1 µm DNA is composed of ∼2.59 kb (Jackson and Pombo, 1998), and nucleotide incorporation lasted for 30 min.

Generation of stable cell lines

U2OS FIT cells (and U2OS FIT ISG15/KO cells) carrying EV, FLAG-ISG15, or FLAG-ISG15ΔGG were generated by Flp recombinase–mediated integration (Thermo Fisher Scientific; Flp-In T-REx Core Kit, catalog number K650001). Briefly, cells were transfected with pcDNA5 EV, pcDNA5 FLAG-ISG15, or pcDNA5 FLAG-ISG15ΔGG using FuGENE Transfection Reagent together with pOG44 vector (Thermo Fisher Scientific; catalog number V600520; 9:1 pOG44/pcDNA5) and 48 h after transfection selected for 2 wk with hygromycin B. Single clones were isolated in plate with cloning cylinders and expanded. *ISG15* expression was tested by immunofluorescence after 48 h of doxycycline (1 µg/ml). Five clones that were comparable in ISG15 expression were pooled together and used for experiments where we referred to them as EV, ISG15, and ISG15ΔGG. MCF7 ISG15/KO cells were transfected with pcDNA3.1 empty, pcDNA3.1 FLAG-ISG15 using FuGENE Transfection Reagent. 24 h after transfection, antibiotic Geneticin (800 µg/ml) was added onto the cells to select cells that randomly integrated the vector in the genome.

Flow cytometer analysis of EdU incorporation

Cells were labeled for 30 min with 10 µM EdU, harvested, and fixed for 10 min in 4% formaldehyde/PBS. Cells were blocked for 15 min with 1% BSA/PBS, pH 7.4. Incorporated EdU was labeled with click reaction according to the manufacturer's instructions (Thermo Fisher Scientific; Click-iT Plus EdU Cell Proliferation Kit for Imaging, catalog number C10640). Total DNA was stained with 1 µg/ml DAPI. Samples were treated for 15 min with 100 µg/ml RNaseA and analyzed on an Attune NxT Flow Cytometer (Thermo Fisher Scientific) and analyzed using FlowJo software V.10.0.8 (FlowJo).

Immunoblotting

Whole-cell extracts were prepared in lysis buffer 1% SDS and 50 mM Tris-HCl, pH 8.0, prewarmed at 95°C. After sonication and clearing (15 min, 16,000 rcf), lysates were analyzed by SDS-PAGE. 20 µg protein was solved in 8% or 12% acrylamide gel and transferred onto a nitrocellulose membrane. The following antibodies were used for immunoblotting: human-ISG15 1:1,000 (provided by K.P. Knobeloch), RECQ1 1:40,000 (Bethyl Laboratories; catalog number A300-450A), FLAG M2 1:1,000

(Sigma-Aldrich; catalog number F3166), pSTAT1 (Tyr701) 1:1,000 (Cell Signaling; catalog number 7649), STAT1 p84/p91 1:1,000 (Santa Cruz; catalog number sc-464), tubulin 1:8,000 (Sigma-Aldrich), Lamin A 1:1,000 (Sigma-Aldrich; catalog number L1293), GAPDH 1:50,000 (Millipore; catalog number MAB374), H3 1:5,000 (Abcam; catalog number ab1791), PCNA 1:1,000 (Santa Cruz; catalog number sc-56), and myc (9E10) 1:1,000 (Santa Cruz; catalog number sc-40).

Immunoprecipitation and mass spectrometry analysis

Chromatin fractions, prepared as above without the sonication step, were extracted from U2OS FIT cells expressing the EV or FLAG-ISG15ΔGG (72 h of doxycycline induction, 1 µg/ml). 2 mg chromatin fractions were incubated for 2 h 4°C on a wheel with anti-FLAG resins (Sigma-Aldrich; catalog number A2220). Resins were washed four times with HNTG buffer (20 mM Hepes, pH 7.5, 150 mM NaCl, 10% glycerol, and 0.1% Triton X-100) before elution with 0.1 M glycine (pH 2.2) for 5 min on ice. Eluted samples were precipitated in 10% TCA and washed twice with cold acetone. Dry pellets were dissolved in a buffer containing 10 mM Tris and 2 mM $CaCl_2$, pH 8.2, and then 0.5 µg of trypsin was added. After digestion, samples were dried, dissolved in 20 µl 0.1% formic acid, and subjected to liquid chromatography with tandem mass spectrometry (LC/MS/MS) at the Functional Genomic Center Zurich. All MS/MS samples were analyzed using Mascot (Matrix Science, London, UK; version 2.5.1.3). Mascot was set up to search the SwissProt_autoup_20180912 database (selected for *Homo sapiens*, unknown version, 20,395 entries). Mascot was searched with a fragment ion mass tolerance of 0.030 D and a parent ion tolerance of 10.0 PPM. Oxidation of methionine was specified in Mascot as a variable modification. Scaffold (Proteome Software; version Scaffold_4.8.9) was used to validate MS/MS based peptide and protein identifications. Peptide identifications were accepted if they could be established at greater than 21.0% probability to achieve a false discovery rate (FDR) less than 0.1% by the Scaffold Local FDR algorithm. Protein identifications were accepted if they could be established at greater than 94.0% probability to achieve an FDR <1.0% and contained at least two identified peptides. Protein probabilities were assigned by the Protein Prophet algorithm (Nesvizhskii et al., 2003). Proteins that contained similar peptides and could not be differentiated based on MS/MS analysis alone were grouped to satisfy the principles of parsimony. Proteins sharing significant peptide evidence were grouped into clusters.

IFN-β stimulation

U2OS FIT and MCF7 cells were treated for 2 h in complete media complemented with 30 U/ml IFN-β (PeproTech; catalog number 300-02BC), washed with warm PBS, and released in fresh media for 46 h unless otherwise explained; ISG15 induction and IFN-β activity (phosphorylation of Tyr 701 of STAT1, pSTAT1; Cell Signaling; catalog number 7649) were tested by immunoblotting.

ISGylation machinery transfection

HEK293T cells were transfected with calcium phosphate using 2 µg pcDNA3 carrying EV, FLAG-ISG15 WT, or FLAG-ISG15 mutants (ΔGG, L72A, LLVAAA) with or without ISGylation machinery components: 4 µg UBE1L (E1), 2 µg of UBCH8 (E2), and 4 µg HERC5 (E3) and then collected for Western blot analysis after 48 h.

iPOND

iPOND was performed as previously described (Sirbu et al., 2011). Briefly, exponentially growing cells HEK293T cells were transfected with EV or myc-ISG15 with calcium phosphate. After 48 h, cells were incubated for 10 min with 10 µM EdU, cross-linked with 1% formaldehyde, harvested, and permeabilized. For thymidine-chase controls (Thy-chase), cells were incubated for 10 min in 10 µM EdU, washed and incubated for 1 h with medium containing 10 µM thymidine, and then cross-linked for 5 min with 1% formaldehyde in PBS. Biotin azide was covalently attached to EdU within newly replicated DNA using Click reaction, and EdU-containing DNA was precipitated using streptavidin–agarose beads (Millipore; catalog number 69203). EdU coprecipitates were boiled in Laemmli buffer and then analyzed by immunoblotting.

Metaphase spreading

Asynchronously and subconfluent cells were incubated for 16 h in fresh medium containing 200 ng/ml nocodazole. Cells were collected by trypsinization and swollen for 20 min at 37°C with 75 mM KCl. The swollen mitotic cells were fixed in 3:1 methanol/acetic acid solution and subsequently spread dropwise onto prehydrated glass microscopy slides and air-dried overnight. The slides were mounted the following day using VECTASHIELD Antifade Mounting Medium with DAPI. Images of randomly selected metaphases were acquired by Leica DM6 B upright digital microscope equipped with a DFC360 FX Leica camera. Images were analyzed using ImageJ64, and chromatid breaks/gaps were counted.

NanoBRET

HEK293T cells were cotransfected with HaloTag-Fusion construct (2 µg; Promega) and varying concentrations of Nluc-fusion vector (MDM2, 200 ng; RECQ1, 20 ng; Promega). After 20 h, cells were mixed with the HaloTag binding ligand 618 and replated 2×10^4 cells per well on a white flat-bottom 96-well plate and incubated for 18–24 h. Luciferase substrate was added (Furimazine) to each well, and then Luminescence signal (counts/second) was measured using the Tecan Spark Machine. NanoBRET ratio was calculated by dividing the acceptor signal by the donor signal. Subsequently, the no-ligand control was subtracted from the ligand sample.

Neutral comet assay

U2OS FIT were induced for 7 d with doxycycline 1 µg/ml and treated for 1 h with 50 nM CPT and washout (3 h). Cells were collected and resuspended in cold PBS. 2×10^4 cells were mixed with 0.8% wt/vol low melting point, previously equilibrated to 37°C, and then spread onto a comet slide (Trevigen; CometAssay Kit, catalog number 4250–050-ESK). Slides were incubated for 20 min at 4°C to allow solidification of the low melting point. Cells were lysed overnight in lysis buffer (Trevigen). Slides were

incubated in cold electrophoresis buffer (300 mM sodium acetate and 100 mM Tris, pH 8.3) for 1 h at 4°C and then subjected to electrophoresis for 30 min at 21 V/300 mA. Samples were rinsed twice in water, fixed in 70% ethanol for 20 min at 4°C, and then dried at 37°C. DNA was stained with SYBR Gold (Thermo Fisher Scientific). Microscopy was performed on a Leica DM6 B upright digital research microscope equipped with a DFC360 FX Leica camera at 10× magnification. The images were analyzed using the Open Comet plugin (http://www.cometbio.org) for Fiji.

PLA

FIT cells were induced 48 h with doxycycline (1 µg/ml) and grown on sterile 12-mm diameter glass coverslip, washed with cold PBS, and preextracted and fixed in 100% cold MeOH for 10 min. After washing three times with PBS, cells were permeabilized for 10 min at room temperature in 0.3% Triton X-100 in PBS and washed twice in PBS. Coverslips were then incubated with primary antibodies overnight: FLAG 1:1,000 (Sigma-Aldrich; catalog number F7425), PCNA 1:100 (Santa Cruz; catalog number sc-56), ISG15 1:1,000 (kindly provided by K.P. Knobeloch, Freiburg, Germany), and RECQ1 (A-9) 1:500 (Santa Cruz; catalog number sc-166388). 25 µM EdU was added to media for 10 min before fixing (10 min) MeOH and permeabilizing (10 min) with 0.3% Triton X-100; EdU was linked to biotin-NaN3 with click chemistry and then immunolabeled with anti-BIOTIN antibody Mo 1:500 (Jackson ImmunoResearch, Catalog number 200–002-211). After PBS washes, cells were incubated with mouse PLUS probe (Sigma-Aldrich, Catalog number DUO82001) and rabbit MINUS probe (Sigma-Aldrich; catalog number DUO82005) for 1 h at 37°C. Ligation was performed in ligation buffer (Sigma-Aldrich; catalog number DUO82009-1000Rxn) with Ligase (Sigma-Aldrich; catalog number DUO82027-1EA) for 30 min at 37°C and followed by amplification using Amplification Buffer Far Red (Sigma-Aldrich; catalog number DUO82028Rxn) and Polymerase (Sigma-Aldrich; catalog number DUO82028-1EA) for 100 min at 37°C. Cells were then washed with 0.2 M Tris, 0.1 M NaCl buffer and incubate for 15 min at RT with DAPI (0.5 µg/ml). Coverslips were mounted using ProLong Gold Antifade Reagent.

QIBC

Automated multichannel wide-field microscopy for quantitative image-based cytometry (QIBC) was performed on an Olympus ScanR Screening System equipped with wide-field optics, a UPLSAPO 20× (0.75 NA), an inverted motorized Olympus IX83 microscope, a motorized stage, infrared (IR)-laser hardware autofocus, a fast emission filter wheel with single-band emission filters, and a 12-bit digital monochrome Hamamatsu ORCA-FLASH 4.0 V2 sCMOS (scientific complementary metal–oxide–semiconductor) camera (2,048 × 2,048 pixels). Images containing ≥1,000 cells per condition were acquired under nonsaturating conditions, and identical settings were applied to all samples within one experiment. Images were processed and analyzed with the inbuilt Olympus ScanR Image Analysis Software (version 3.0.0), a dynamic background correction was applied, nuclei segmentation was performed using an integrated intensity-based object detection module using the DAPI signal, and foci segmentation was performed using an integrated spot-detection module. Fluorescence intensities were quantified and are depicted as arbitrary units. These values were exported and analyzed with Spotfire data visualization software (TIBCO software version 7.0.1; https://www.tibco.com/products/tibco-spotfire). Within one experiment, similar cell numbers were compared for the different conditions. To visualize discrete data in scatterplots, mild jittering was applied to demerge overlapping data points. Representative scatterplots and quantifications of independent experiments are shown.

siRNA knockdown

Cells were plated and transfected the following day with siRNA oligonucleotides targeting *ISG15* (5′-GCAACGAAUUCCAGGUGUC-3′), RECQ1 (5′-UUACCAGUUACCAGCAUUAUUdTdT-3′), or luciferase (5′-CUUACGCUGAGUACUUCGAdTdT-3′) at a final concentration of 40 nM. Transfections were performed using JetPRIME according to the manufacturer's instruction 48 h after transfection for *ISG15* knockdown. For *RECQ1* knockdown, transfection was repeated after 24 h. Transfection medium was replaced with complete medium after 24 h and protein depletion confirmed 48 h after the second transfection by immunoblotting.

Site-specific mutagenesis

pcDNA3.1 FLAG-ISG15 was mutagenized using the following primers: L10A forward, 5′-GACCTGACGGTGAAGATGGCGGCGGGCAACGAATTCC-3′; L10A reverse, 5′-GGAATTCGTTGCCCGCCGCCATCTTCACCGTCAGGTC-3′; L72A forward, 5′-GGCCCCGGCAGCACGGTCGCGCTGGTGGTGGACAAATG-3′; L72A reverse, 5′-CATTTGTCCACCACCAGCGCGACCGTGCTGCCGGGGCC-3′; V74A forward, 5′-GGCAGCACGGTCCTGCTGGCGGTGGACAAATGCGACG-3′; and V74A reverse, 5′-CGTCGCATTTGTCCACCGCCAGCAGGACCGTGCTGCC-3′; pcDNA3.1 FLAG-ISG15L10A was mutagenized using the following primers: 3X forward, 5′-GGCAGCACGGTCGCGCTGGCGGTGGACAAATGCGACG-3′; 3X reverse, 5′-CGTCGCATTTGTCCACCGCCAGCGCGACCGTGCTGCC-3′. PfuTurbo DNA polymerase (Agilent Technologies; Pfu, catalog number 600250) was used for the reaction and checked on a 0.8% agarose gel. Template was digested with 1 µl DpnI (New England Biolabs; catalog number R0176S) and TOP10 (bacteria; Thermo Fisher Scientific; catalog number C4040-03) were transformed with mutagenized vector overnight at 37°C. Mutated vectors were sequenced using cytomegalovirus (CMV) primer (5′-CGCAAATGGGCGGTAGGCGTG-3′).

Survival assay

Cells were seeded in 96-well plate and treated the day after with the genotoxic agents CPT (1, 5, 25, 50, and 150 nM) and Olaparib (0.5, 1, 5, and 10 µM) for 7 to 10 d. Resulting colonies were fixed with 100% cold MeOH and stained with 0.05% crystal violet in 100% MeOH for up to 2 h. Excess was washed out and cells were destained for 30 min with MeOH. Crystal violet in suspension was analyzed by measuring the absorbance at 600 nm using SpectraMaxi3.

Statistics

The number of forks (fiber assay), nuclei (comet assay) or metaphase scored in the shown replicate and number of

biological replicates is defined in the figure legends. Results were analyzed in GraphPad using a Mann–Whitney *U* test (two-tailed P value; P value > 0.05 was considered not significant). Flow cytometry data were analyzed using FlowJo software V.10.0.8 (https://www.flowjo.com/). The intensity values of EdU-positive cells per sample were extracted from the raw data and subjected to statistical analysis using GraphPad Prism 7 (two-tailed P value). In the neutral comet assay, double strands were evaluated measuring Olive tail moment (Olive moment), a parameter that includes the tail length and the fraction of total DNA in the tail, using the Open Comet plugin (http://www.cometbio.org/) for Fiji. The results were analyzed using GraphPad Prism7 using a Mann–Whitney test. Results were displayed as scatterplots with mean and SD. In the clonogenic assay, absorbance of each sample (technical triplicate) was normalized on untreated samples and on the corresponding treated EV sample.

Online supplemental material

Fig. S1 shows the pipeline for the generation of the *ISG15* KO, analysis of representative clones in U2OS, and additional experiments on the ISG15 localization at the replication forks and the effect of its deregulated expression on DNA synthesis. Fig. S2 shows analysis of representative *ISG15* KO clones in MCF7 and expression of ISG15 in different cancer cell lines. Fig. S3 reports additional experiments on the effect of the expression of the conjugation-defective form of ISG15 (ISG15ΔGG) in DNA synthesis and cell cycle profile, as well as a sequence alignment of human ISG15 and ubiquitin and further characterization of the ISG15 mutants tested in the replication phenotype. Fig. S4 shows the immunoprecipitation experiment performed for mass spectrometry studies, additional details of the ISG15–RECQ1 interaction, and the detrimental effects of expression of ISG15 and ISG15ΔGG in DNA replication fork progression and DNA damage upon a mild dose of replication stress. Table S1 reports the interacting factors identified by mass spectrometry.

Acknowledgments

We thank Massimo Lopes for critical reading of the manuscript and all members of Penengo and Lopes laboratories for technical support and helpful discussions, Jana Krietsch and Davide Eletto for helping with cell sorting and screen of KO cell lines, Alessandro Vindigni (Washington University, St. Louis, MO) for providing RECQ1 constructs, and the Functional Genomic Center of the University of Zurich for mass spectrometry analysis.

This work was supported by Helmut Horten Stiftung, Krebsliga Schweiz (KFS-4577-08-2018), and Swiss National Science Foundation research grants 310030_184966 and 31003A_166370 to L. Penengo.

The authors declare no competing financial interests.

Author contributions: M.C. Raso performed DNA fiber experiments, metaphase spreads, and comet and survival assays; M.C. Raso and N. Djoric generated the ISG15 KO cell lines and performed iPOND and cell fractionation and PLA studies; M.C. Raso performed the statistical analysis and contributed to the experimental design; F. Walser performed QIBC analysis; F.M. Schmid prepared samples for the mass spectrometry analysis; S. Burger for technical assistance; S. Hess and K.-P. Knobeloch performed the NanoBRET analysis; and L. Penengo conceived the project, designed experiments, and wrote the manuscript, supported by M.C. Raso.

Submitted: 16 April 2020
Revised: 27 April 2020
Accepted: 4 May 2020

References

Andersen, J.B., M. Aaboe, E.C. Borden, O.G. Goloubeva, B.A. Hassel, and T.F. Orntoft. 2006. Stage-associated overexpression of the ubiquitin-like protein, ISG15, in bladder cancer. *Br. J. Cancer*. 94:1465–1471. https://doi.org/10.1038/sj.bjc.6603099

Bektas, N., E. Noetzel, J. Veeck, M.F. Press, G. Kristiansen, A. Naami, A. Hartmann, A. Dimmler, M.W. Beckmann, R. Knüchel, et al. 2008. The ubiquitin-like molecule interferon-stimulated gene 15 (ISG15) is a potential prognostic marker in human breast cancer. *Breast Cancer Res*. 10: R58. https://doi.org/10.1186/bcr2117

Berti, M., and A. Vindigni. 2016. Replication stress: getting back on track. *Nat. Struct. Mol. Biol*. 23:103–109. https://doi.org/10.1038/nsmb.3163

Berti, M., A. Ray Chaudhuri, S. Thangavel, S. Gomathinayagam, S. Kenig, M. Vujanovic, F. Odreman, T. Glatter, S. Graziano, R. Mendoza-Maldonado, et al. 2013. Human RECQ1 promotes restart of replication forks reversed by DNA topoisomerase I inhibition. *Nat. Struct. Mol. Biol*. 20:347–354. https://doi.org/10.1038/nsmb.2501

Brown, J.S., and S.P. Jackson. 2015. Ubiquitylation, neddylation and the DNA damage response. *Open Biol*. 5. 150018. https://doi.org/10.1098/rsob.150018

Burks, J., R.E. Reed, and S.D. Desai. 2014. ISGylation governs the oncogenic function of Ki-Ras in breast cancer. *Oncogene*. 33:794–803. https://doi.org/10.1038/onc.2012.633

Chiang, T.W., C. le Sage, D. Larrieu, M. Demir, and S.P. Jackson. 2016. CRISPR-Cas9(D10A) nickase-based genotypic and phenotypic screening to enhance genome editing. *Sci. Rep*. 6:24356. https://doi.org/10.1038/srep24356

Coquel, F., M.J. Silva, H. Técher, K. Zadorozhny, S. Sharma, J. Nieminuszczy, C. Mettling, E. Dardillac, A. Barthe, A.L. Schmitz, et al. 2018. SAMHD1 acts at stalled replication forks to prevent interferon induction. *Nature*. 557:57–61. https://doi.org/10.1038/s41586-018-0050-1

D'Cunha, J., S. Ramanujam, R.J. Wagner, P.L. Witt, E. Knight, Jr., and E.C. Borden. 1996. In vitro and in vivo secretion of human ISG15, an IFN-induced immunomodulatory cytokine. *J. Immunol*. 157:4100–4108.

Dantuma, N.P., and H. van Attikum. 2016. Spatiotemporal regulation of posttranslational modifications in the DNA damage response. *EMBO J*. 35:6–23. https://doi.org/10.15252/embj.201592595

Desai, S.D., A.L. Haas, L.M. Wood, Y.C. Tsai, S. Pestka, E.H. Rubin, A. Saleem, A. Nur-E-Kamal, and L.F. Liu. 2006. Elevated expression of ISG15 in tumor cells interferes with the ubiquitin/26S proteasome pathway. *Cancer Res*. 66:921–928. https://doi.org/10.1158/0008-5472.CAN-05-1123

Desai, S.D., L.M. Wood, Y.C. Tsai, T.S. Hsieh, J.R. Marks, G.L. Scott, B.C. Giovanella, and L.F. Liu. 2008. ISG15 as a novel tumor biomarker for drug sensitivity. *Mol. Cancer Ther*. 7:1430–1439. https://doi.org/10.1158/1535-7163.MCT-07-2345

Desai, S.D., R.E. Reed, J. Burks, L.M. Wood, A.K. Pullikuth, A.L. Haas, L.F. Liu, J.W. Breslin, S. Meiners, and S. Sankar. 2012. ISG15 disrupts cytoskeletal architecture and promotes motility in human breast cancer cells. *Exp. Biol. Med. (Maywood)*. 237:38–49. https://doi.org/10.1258/ebm.2011.011236

Dos Santos, P.F., and D.S. Mansur. 2017. Beyond ISGlylation: Functions of Free Intracellular and Extracellular ISG15. *J. Interferon Cytokine Res*. 37: 246–253. https://doi.org/10.1089/jir.2016.0103

Forment, J.V., and M.J. O'Connor. 2018. Targeting the replication stress response in cancer. *Pharmacol. Ther*. 188:155–167. https://doi.org/10.1016/j.pharmthera.2018.03.005

Forys, J.T., C.E. Kuzmicki, A.J. Saporita, C.L. Winkeler, L.B. Maggi, Jr., and J.D. Weber. 2014. ARF and p53 coordinate tumor suppression of an oncogenic IFN-β-STAT1-ISG15 signaling axis. *Cell Rep*. 7:514–526. https://doi.org/10.1016/j.celrep.2014.03.026

Gogola, E., A.A. Duarte, J.R. de Ruiter, W.W. Wiegant, J.A. Schmid, R. de Bruijn, D.I. James, S.G. Llobet, D.J. Vis, S. Annunziato, et al. 2019.

Selective Loss of PARG Restores PARylation and Counteracts PARP Inhibitor-Mediated Synthetic Lethality. *Cancer Cell*. 35:950–952. https://doi.org/10.1016/j.ccell.2019.05.012

Hadjivasiliou, A.. 2012. ISG15 implicated in cytoskeleton disruption and promotion of breast cancer. *Expert Rev. Proteomics*. 9:7.

Han, H.G., H.W. Moon, and Y.J. Jeon. 2018. ISG15 in cancer: Beyond ubiquitin-like protein. *Cancer Lett*. 438:52–62. https://doi.org/10.1016/j.canlet.2018.09.007

Hicke, L., H.L. Schubert, and C.P. Hill. 2005. Ubiquitin-binding domains. *Nat. Rev. Mol. Cell Biol*. 6:610–621. https://doi.org/10.1038/nrm1701

Ina, S., S. Hirono, T. Noda, and H. Yamaue. 2010. Identifying molecular markers for chemosensitivity to gemcitabine in pancreatic cancer: increased expression of interferon-stimulated gene 15 kd is associated with intrinsic chemoresistance. *Pancreas*. 39:473–485. https://doi.org/10.1097/MPA.0b013e3181c0decc

Jackson, D.A., and A. Pombo. 1998. Replicon clusters are stable units of chromosome structure: evidence that nuclear organization contributes to the efficient activation and propagation of S phase in human cells. *J. Cell Biol*. 140:1285–1295. https://doi.org/10.1083/jcb.140.6.1285

Jeon, Y.J., M.G. Jo, H.M. Yoo, S.H. Hong, J.M. Park, S.H. Ka, K.H. Oh, J.H. Seol, Y.K. Jung, and C.H. Chung. 2012. Chemosensitivity is controlled by p63 modification with ubiquitin-like protein ISG15. *J. Clin. Invest*. 122:2622–2636. https://doi.org/10.1172/JCI61762

Jinawath, N., Y. Furukawa, S. Hasegawa, M. Li, T. Tsunoda, S. Satoh, T. Yamaguchi, H. Imamura, M. Inoue, H. Shiozaki, et al. 2004. Comparison of gene-expression profiles between diffuse- and intestinal-type gastric cancers using a genome-wide cDNA microarray. *Oncogene*. 23:6830–6844. https://doi.org/10.1038/sj.onc.1207886

Kerscher, O., R. Felberbaum, and M. Hochstrasser. 2006. Modification of proteins by ubiquitin and ubiquitin-like proteins. *Annu. Rev. Cell Dev. Biol*. 22:159–180. https://doi.org/10.1146/annurev.cellbio.22.010605.093503

Laljee, R.P., S. Muddaiah, B. Salagundi, P.M. Cariappa, A.S. Indra, V. Sanjay, and A. Ramanathan. 2013. Interferon stimulated gene-ISG15 is a potential diagnostic biomarker in oral squamous cell carcinomas. *Asian Pac. J. Cancer Prev*. 14:1147–1150. https://doi.org/10.7314/APJCP.2013.14.2.1147

Li, C., J. Wang, H. Zhang, M. Zhu, F. Chen, Y. Hu, H. Liu, and H. Zhu. 2014. Interferon-stimulated gene 15 (ISG15) is a trigger for tumorigenesis and metastasis of hepatocellular carcinoma. *Oncotarget*. 5:8429–8441. https://doi.org/10.18632/oncotarget.2316

Liu, M., B.T. Hummer, X. Li, and B.A. Hassel. 2004. Camptothecin induces the ubiquitin-like protein, ISG15, and enhances ISG15 conjugation in response to interferon. *J. Interferon Cytokine Res*. 24:647–654. https://doi.org/10.1089/jir.2004.24.647

Loeb, K.R., and A.L. Haas. 1992. The interferon-inducible 15-kDa ubiquitin homolog conjugates to intracellular proteins. *J. Biol. Chem*. 267:7806–7813.

Lou, Z., J. Wei, H. Riethman, J.A. Baur, R. Voglauer, J.W. Shay, and W.E. Wright. 2009. Telomere length regulates ISG15 expression in human cells. *Aging (Albany NY)*. 1:608–621. https://doi.org/10.18632/aging.100066

Macheret, M., and T.D. Halazonetis. 2015. DNA replication stress as a hallmark of cancer. *Annu. Rev. Pathol*. 10:425–448. https://doi.org/10.1146/annurev-pathol-012414-040424

Machleidt, T., C.C. Woodroofe, M.K. Schwinn, J. Méndez, M.B. Robers, K. Zimmerman, P. Otto, D.L. Daniels, T.A. Kirkland, and K.V. Wood. 2015. NanoBRET--A Novel BRET Platform for the Analysis of Protein-Protein Interactions. *ACS Chem. Biol*. 10:1797–1804. https://doi.org/10.1021/acschembio.5b00143

Maya-Mendoza, A., P. Moudry, J.M. Merchut-Maya, M. Lee, R. Strauss, and J. Bartek. 2018. High speed of fork progression induces DNA replication stress and genomic instability. *Nature*. 559:279–284. https://doi.org/10.1038/s41586-018-0261-5

Muñoz, S., and J. Méndez. 2017. DNA replication stress: from molecular mechanisms to human disease. *Chromosoma*. 126:1–15. https://doi.org/10.1007/s00412-016-0573-x

Narasimhan, J., M. Wang, Z. Fu, J.M. Klein, A.L. Haas, and J.J. Kim. 2005. Crystal structure of the interferon-induced ubiquitin-like protein ISG15. *J. Biol. Chem*. 280:27356–27365. https://doi.org/10.1074/jbc.M502814200

Nesvizhskii, A.I., A. Keller, E. Kolker, and R. Aebersold. 2003. A Statistical Model for Identifying Proteins by Tandem Mass Spectrometry. *Anal. Chem*. 75(17):4646–4658.

Padovan, E., L. Terracciano, U. Certa, B. Jacobs, A. Reschner, M. Bolli, G.C. Spagnoli, E.C. Borden, and M. Heberer. 2002. Interferon stimulated gene 15 constitutively produced by melanoma cells induces e-cadherin expression on human dendritic cells. *Cancer Res*. 62:3453–3458.

Park, J.M., S.W. Yang, K.R. Yu, S.H. Ka, S.W. Lee, J.H. Seol, Y.J. Jeon, and C.H. Chung. 2014. Modification of PCNA by ISG15 plays a crucial role in termination of error-prone translesion DNA synthesis. *Mol. Cell*. 54:626–638. https://doi.org/10.1016/j.molcel.2014.03.031

Park, J.H., S.W. Yang, J.M. Park, S.H. Ka, J.H. Kim, Y.Y. Kong, Y.J. Jeon, J.H. Seol, and C.H. Chung. 2016. Positive feedback regulation of p53 transactivity by DNA damage-induced ISG15 modification. *Nat. Commun*. 7:12513. https://doi.org/10.1038/ncomms12513

Perng, Y.C., and D.J. Lenschow. 2018. ISG15 in antiviral immunity and beyond. *Nat. Rev. Microbiol*. 16:423–439. https://doi.org/10.1038/s41579-018-0020-5

Popuri, V., C.Z. Bachrati, L. Muzzolini, G. Mosedale, S. Costantini, E. Giacomini, I.D. Hickson, and A. Vindigni. 2008. The Human RecQ helicases, BLM and RECQ1, display distinct DNA substrate specificities. *J. Biol. Chem*. 283:17766–17776. https://doi.org/10.1074/jbc.M709749200

Quinet, A., D. Lemaçon, and A. Vindigni. 2017. Replication Fork Reversal: Players and Guardians. *Mol. Cell*. 68:830–833. https://doi.org/10.1016/j.molcel.2017.11.022

Sharma, S., J.A. Sommers, S. Choudhary, J.K. Faulkner, S. Cui, L. Andreoli, L. Muzzolini, A. Vindigni, and R.M. Brosh, Jr.. 2005. Biochemical analysis of the DNA unwinding and strand annealing activities catalyzed by human RECQ1. *J. Biol. Chem*. 280:28072–28084. https://doi.org/10.1074/jbc.M500264200

Shen, J., J. Wei, H. Wang, G. Yue, L. Yu, Y. Yang, L. Xie, Z. Zou, X. Qian, Y. Ding, et al. 2013. A three-gene signature as potential predictive biomarker for irinotecan sensitivity in gastric cancer. *J. Transl. Med*. 11:73. https://doi.org/10.1186/1479-5876-11-73

Sirbu, B.M., F.B. Couch, J.T. Feigerle, S. Bhaskara, S.W. Hiebert, and D. Cortez. 2011. Analysis of protein dynamics at active, stalled, and collapsed replication forks. *Genes Dev*. 25(12):1320–1327. https://doi.org/10.1101/gad.2053211

Swaim, C.D., A.F. Scott, L.A. Canadeo, and J.M. Huibregtse. 2017. Extracellular ISG15 Signals Cytokine Secretion through the LFA-1 Integrin Receptor. *Mol. Cell*. 68:581–590.e585. https://doi.org/10.1016/j.molcel.2017.10.003

Talvinen, K., J. Tuikkala, J. Grönroos, H. Huhtinen, P. Kronqvist, T. Aittokallio, O. Nevalainen, H. Hiekkanen, T. Nevalainen, and J. Sundström. 2006. Biochemical and clinical approaches in evaluating the prognosis of colon cancer. *Anticancer Res*. 26(6C):4745–4751.

Thangavel, S., M. Berti, M. Levikova, C. Pinto, S. Gomathinayagam, M. Vujanovic, R. Zellweger, H. Moore, E.H. Lee, E.A. Hendrickson, et al. 2015. DNA2 drives processing and restart of reversed replication forks in human cells. *J. Cell Biol*. 208:545–562. https://doi.org/10.1083/jcb.201406100

Villarroya-Beltri, C., S. Guerra, and F. Sánchez-Madrid. 2017. ISGylation - a key to lock the cell gates for preventing the spread of threats. *J. Cell Sci*. 130:2961–2969. https://doi.org/10.1242/jcs.205468

Wang, Z., W.G. Zhu, and X. Xu. 2017. Ubiquitin-like modifications in the DNA damage response. *Mutat. Res*. 803–805:56–75. https://doi.org/10.1016/j.mrfmmm.2017.07.001

Zellweger, R., D. Dalcher, K. Mutreja, M. Berti, J.A. Schmid, R. Herrador, A. Vindigni, and M. Lopes. 2015. Rad51-mediated replication fork reversal is a global response to genotoxic treatments in human cells. *J. Cell Biol*. 208:563–579. https://doi.org/10.1083/jcb.201406099

Zeman, M.K., and K.A. Cimprich. 2014. Causes and consequences of replication stress. *Nat. Cell Biol*. 16:2–9. https://doi.org/10.1038/ncb2897

Zhang, X., D. Bogunovic, B. Payelle-Brogard, V. Francois-Newton, S.D. Speer, C. Yuan, S. Volpi, Z. Li, O. Sanal, D. Mansouri, et al. 2015. Human intracellular ISG15 prevents interferon-α/β over-amplification and auto-inflammation. *Nature*. 517:89–93. https://doi.org/10.1038/nature13801

JCB

Supplemental material

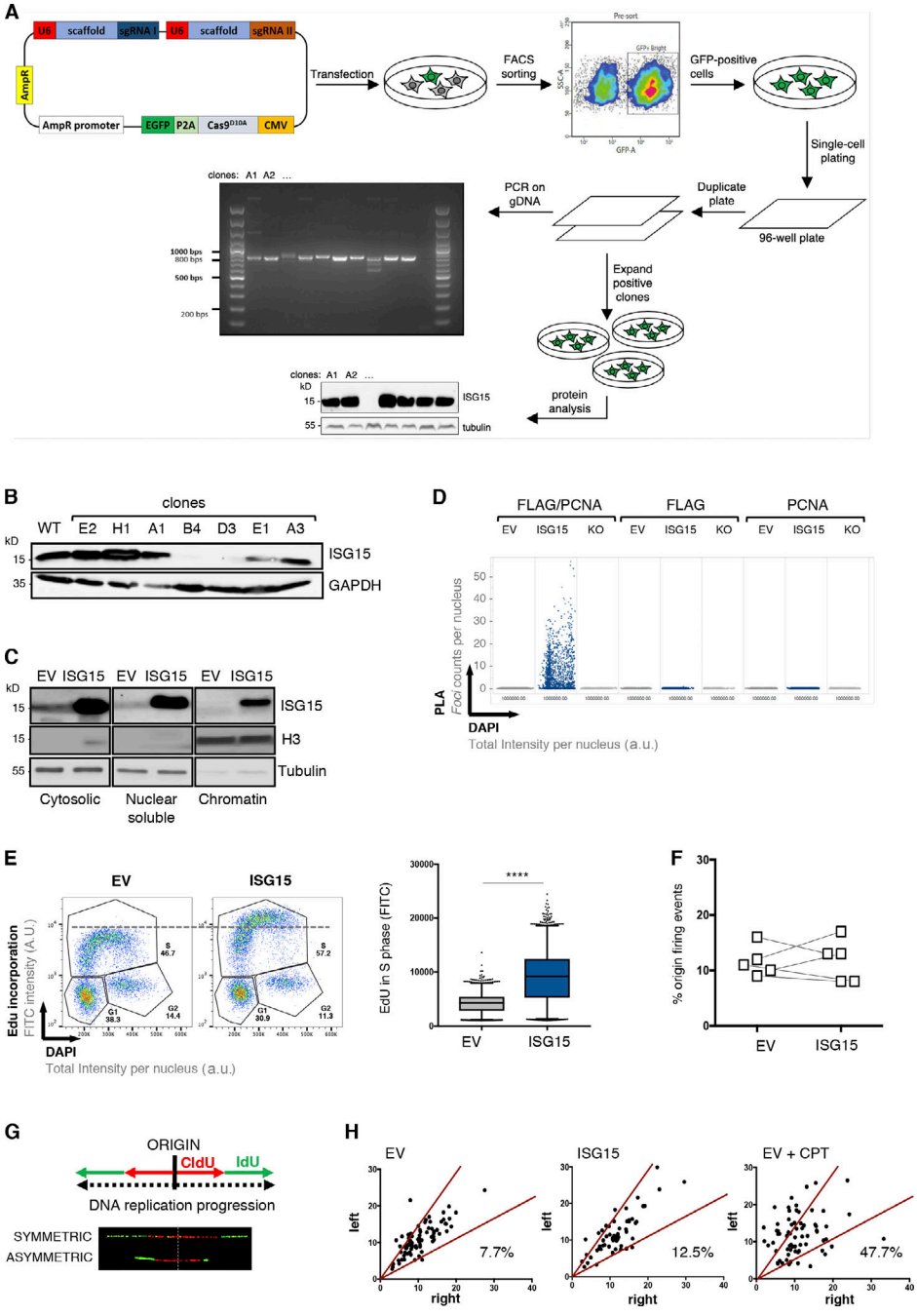

Figure S1. **ISG15 localizes at the DNA replication forks and accelerates replication fork progression. (A)** Schematic representation of the pipeline followed for the generation of CRISPR/Cas9-mediated ISG15 KO cell lines. **(B)** Analysis of ISG15 protein levels in 7 of the 42 single clones tested, obtained from the CRISPR/Cas9 KO in U2OS FIT cells. Clone D3 was selected and used for the following experiments (in the main text referred to as U2OS ISG15/KO). 50 µg cell extracts was analyzed by Western blotting as indicated. **(C)** Subcellular localization of ISG15 in U2OS FIT cells expressing EV or FLAG-ISG15 after 48 h induction with 1 µg/ml doxycycline. Indicated are the different fractions analyzed. **(D)** Quantification of PLA foci counts by automated microscopy (QIBC) of FLAG-ISG15 colocalization with PCNA (FLAG/PCNA) determined by PLA in U2OS FIT cells after induction with 1 µg/ml doxycycline for 48 h. For each condition, images containing ≥1,000 cells per experiment were acquired (n = 3). **(E)** U2OS FIT cells after doxycycline induction (1 µg/ml, 48 h) and grown in media supplemented with 10 µM EdU for 30 min before collecting and processing for FACS analysis. Left: DNA content (DAPI) and DNA synthesis, indicated by EdU incorporation (FITC) measured by FACS. Right: Quantification of EdU incorporation of cells in S phase. Similar results were obtained in at least one independent experiment. **(F)** Percentage of origin firing events in U2OS FIT expressing either the EV or FLAG-ISG15 after doxycycline induction (1 µg/ml, 48 h). Origin firing events were evaluated by fibers assay (IdU-CldU-IdU) scoring ≥200 DNA fibers per experiment; each point indicates a single experiment. The line connects values for EV and FLAG-ISG15 of the same experiment. **(G)** Graphical scheme of sister forks imaging by DNA fiber assay with representative image. **(H)** Sister forks symmetry plot in U2OS FIT cells after doxycycline induction (1 µg/ml, 48 h). U2OS FIT cells expressing EV were treated with CPT (50 nM, 1 h; EV + CPT) as a positive control for asymmetry. Each fork is described by the length of left and right IdU tracks. Red lines define a range of 30% difference between left and right tracks; left > right + 30% and right > left + 30% are considered asymmetric. Similar results were obtained in at least one independent experiment.

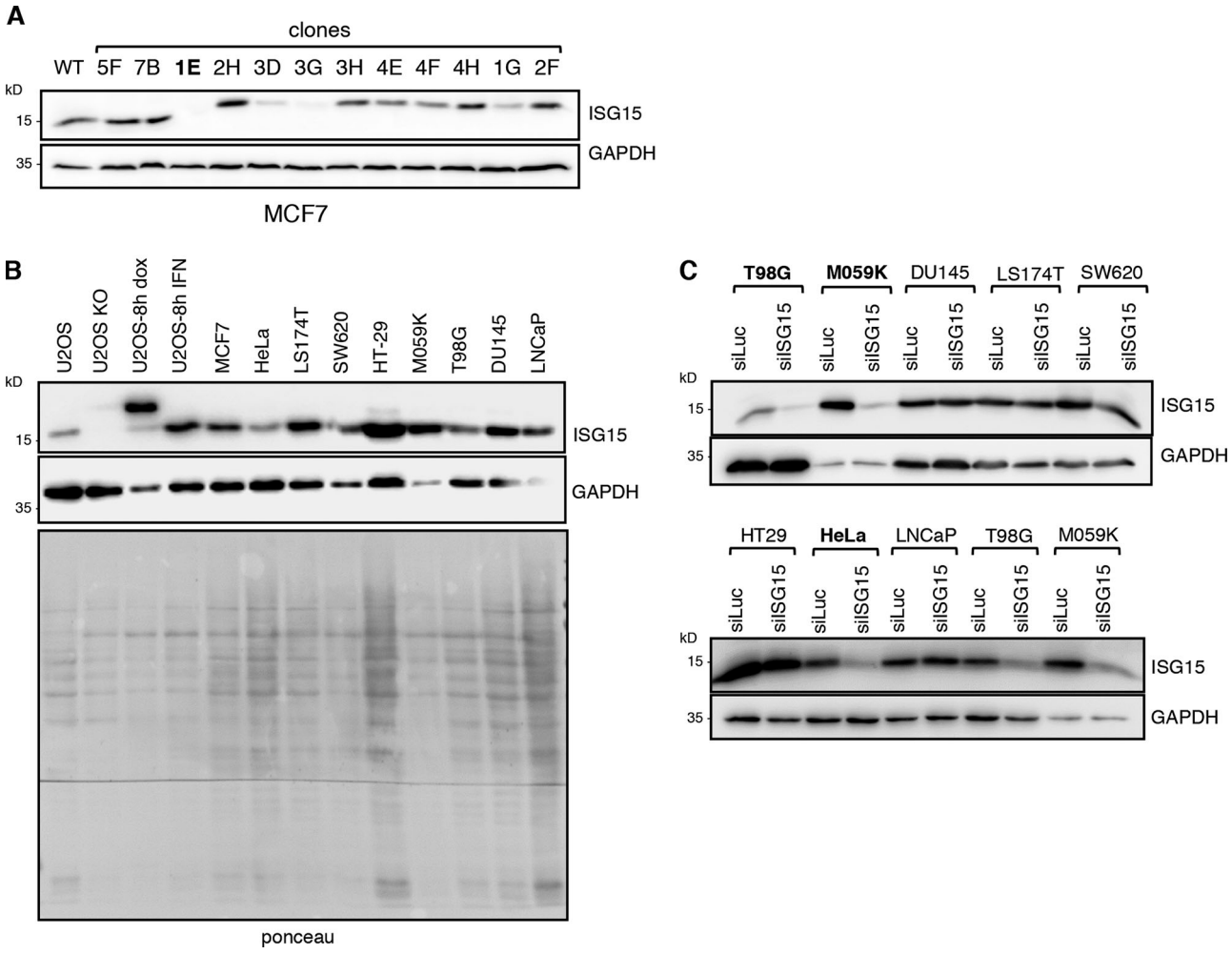

Figure S2. ***ISG15* expression levels impact replication fork progression in different systems. (A)** Analysis of ISG15 protein levels in 12 of the 41 single clones tested, obtained from the CRISPR/Cas9 KO in MCF7 cells. Clone 1E was selected and used for the following experiments (in the main text referred to as MCF7 ISG15/KO). **(B)** ISG15 immunoblot on different cellular system/conditions used in our experiments and several cancer cell lines. HeLa were derived from cervical carcinoma; LS174T, SW620, and HT-29 were derived from colon cancer; M059K and T98G were derived from glioblastoma; DU145 and LNCaP were derived from prostate cancer. **(C)** Test of *ISG15* knockdown efficiency in different cancer cell lines. Cells were transfected with siISG15 or siLuc as a control and collected after 24 h, and ISG15 levels were evaluated by Western blot analysis.

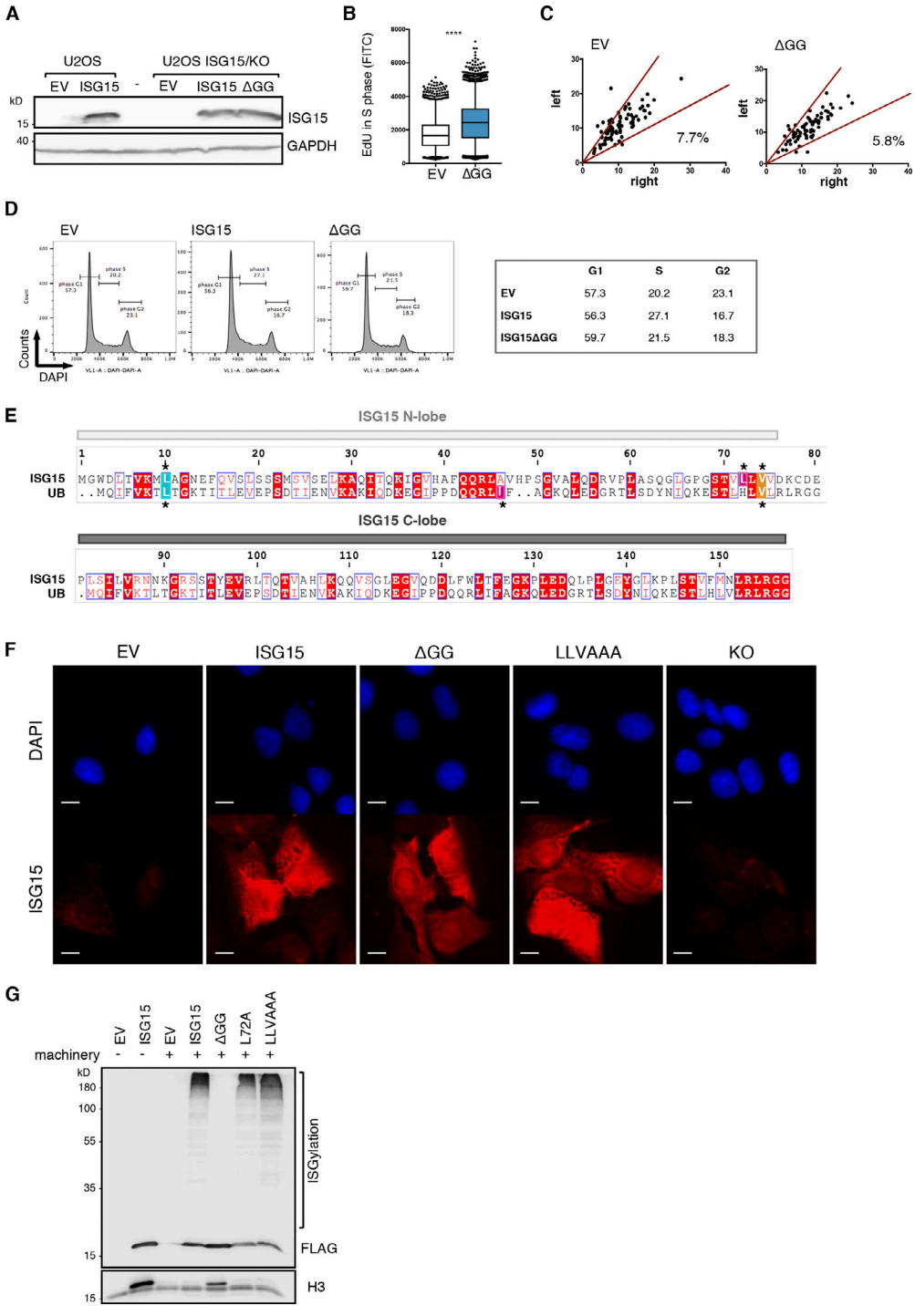

Figure S3. **Accelerated replication fork progression in cells expressing high levels of ISG15 is largely conjugation independent. (A)** ISG15 immunoblot on U2OS FIT cells expressing EV or FLAG-ISG15 and in U2OS FIT cells lacking the endogenous *ISG15* (U2OS ISG15/KO) and reexpressing EV, FLAG-ISG15, or FLAG-ISG15ΔGG after doxycycline induction (1 µg/ml, 48 h). **(B)** Quantification of EdU incorporation in S phase of U2OS FIT cells expressing EV or FLAG-ISG15ΔGG after doxycycline induction (1 µg/ml, 48 h) and grown in the presence of EdU (10 µM for 30 min) before collecting and processing for FACS analysis. Similar results were obtained in at least one independent experiment. **(C)** Fork asymmetry analysis in U2OS FIT expressing EV or FLAG-ISG15ΔGG after doxycycline induction (1 µg/ml, 48 h). Each fork is described by the length of left and right IdU tracks. Red lines define a range of 30% difference between left and right tracks; left > right + 30% and right > left + 30% are considered asymmetric. Similar results were obtained in at least one independent experiment. **(D)** Left: Cell cycle profile of U2OS FIT cells expressing EV, FLAG-ISG15, or FLAG-ISG15ΔGG after 48-h induction with doxycycline. Right: Percentage of cell distribution in different cell cycle phases. **(E)** Sequence alignment of human ISG15 and ubiquitin (UB). The N- and C-lobes are indicated by bars. The conserved residues are in red. The residues that are part of the hydrophobic patch are indicated by asterisks (*). **(F)** Localization of ISG15 in U2OS FIT cells after doxycycline induction (1 µg/ml, 48 h). ISG15 immunostaining was performed after preextraction and MeOH fixation. Scale bars, 10 µm. **(G)** The indicated forms of ISG15 were expressed in HEK293T cells with or without the ISGylation machinery components UBE1L (E1), UBCH8 (E2), and HERC5 (E3). After 48 h, cell extracts were collected for Western blot analysis with the indicated antibodies.

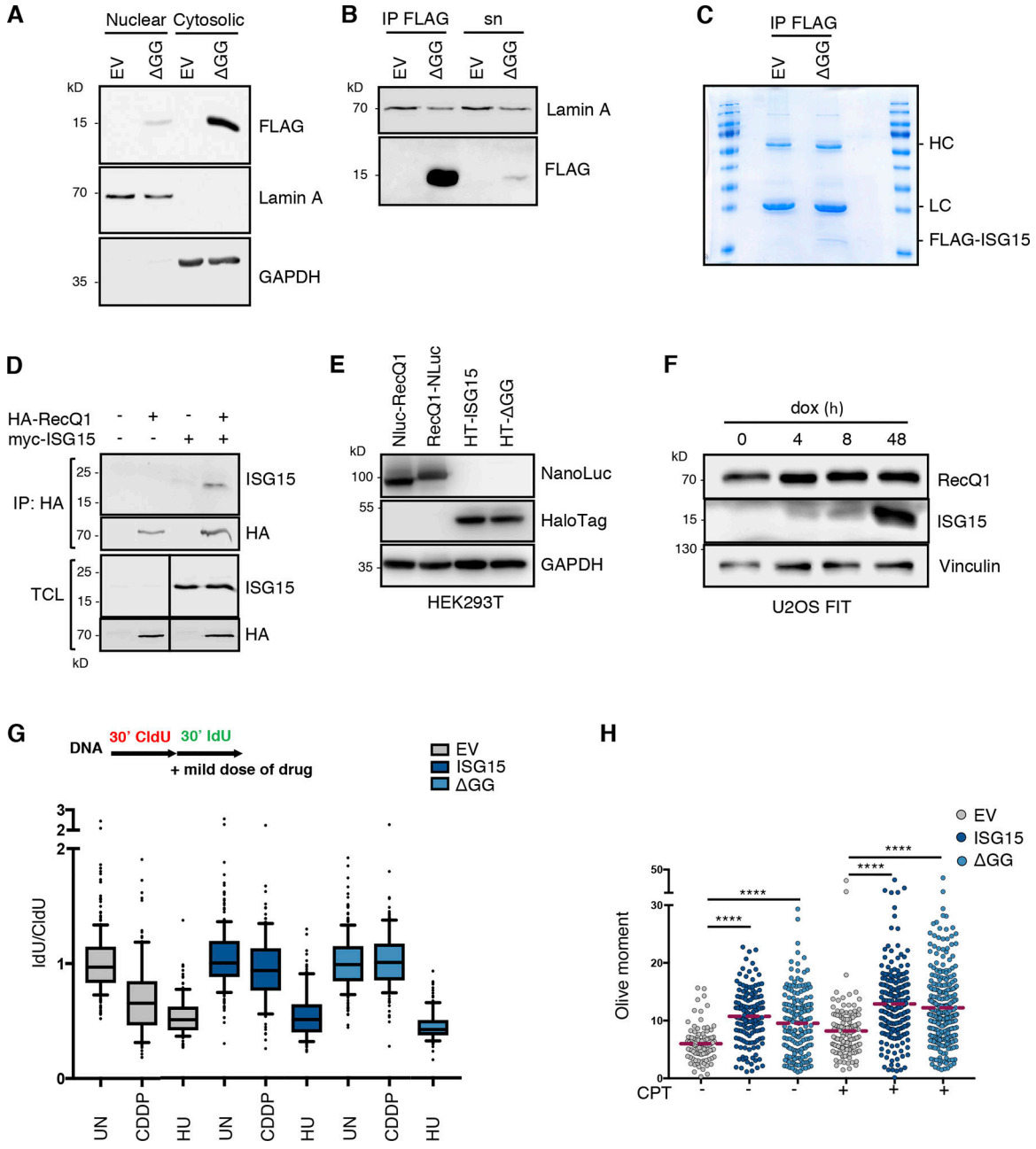

Figure S4. **Increased replication fork progression by ISG15 depends on RECQ1 and leads to unrestrained DNA replication and DNA breakages. (A)** FLAG-immunoblot on protein extracts derived from cytosolic or nuclear fractions of U2OS FIT cells expressing EV or FLAG-ISG15ΔGG. Lamin A and GAPDH are used as controls of fractionation and loading. **(B)** FLAG-ISG15 was immunoprecipitated (IP FLAG) from nuclear extracts as in A and analyzed by FLAG immunoblot. Sn, supernatant after immunoprecipitation. **(C)** FLAG immunoprecipitation as in B, detected by Coomassie blue staining. The band corresponding to FLAG-ISG15ΔGG is indicated. HL and LC represent heavy and light chain of the FLAG antibody, respectively. **(D)** Anti-HA immunoprecipitation from HEK293T cells expressing HA-RecQ1 and myc-ISG15 followed by immunoblot with the indicated antibodies. TCL, total cell extracts. **(E)** HEK293T cells were transfected with 2 µg expression constructs of indicated proteins. Immunoblot was used to detect HaloTag, NanoLuc, and GAPDH. **(F)** RECQ1 protein levels in U2OS FIT expressing FLAG-ISG15 after induction with 1 µg/ml doxycycline (dox) for different time points indicated. Vinculin immunoblot is used as loading control. **(G)** Effect of 1 µM cisplatin (CDDP) or 0.5 mM HU treatment on U2OS FIT cells expressing EV, FLAG-ISG15, or FLAG-ISG15ΔGG after induction with 1 µg/ml doxycycline for 48 h. UN, untreated. Drug effect (IdU + drug) is normalized on CldU track length in untreated conditions. At least 100 tracks were scored per sample (n = 3). **(H)** Neutral comet assay to measure DNA double-strand breaks in U2OS FIT cells expressing EV, FLAG-ISG15, or FLAG-ISG15ΔGG after induction with 1 µg/ml doxycycline for 7 d and treated with 50 nM CPT (n = 3). Statistical analysis according to Mann–Whitney test; ****, $P < 0.0001$.

Table S1 is provided online and shows the identification proteins interacting with ISG15; Y (green) indicates factors associated with chromatin structures, and N (red) indicates factors that are not chromatin associated.